



Nonlinear dynamic responses of beamlike truss based on the equivalent nonlinear beam model

Mei Liu^a, Dengqing Cao^{a,*}, Xiaoyun Zhang^a, Jin Wei^b, Dongfang Zhu^c

^a School of Astronautics, Harbin Institute of Technology, Harbin, 150001, PR China

^b School of Electromechanical and Automotive Engineering, Yantai University, Yantai, 264005, PR China

^c Shanghai Aerospace Control Technology Institute, Shanghai, 201109, PR China



ARTICLE INFO

Keywords:

Equivalent beam model
Beamlike truss
Geometric nonlinearity
Forced vibration
Dynamic response

ABSTRACT

The main goal of this paper is to develop an equivalent nonlinear beam model (ENBM) for forced vibration analysis of the nonlinear beamlike truss (NBT) and its numerical implementation for describing the nonlinear behaviors of the periodic NBT. For the equivalent dynamic modeling method based on the energy equivalence principle of the truss structures, most of the existing approaches focus on studying the linear characteristic which cannot satisfy the nonlinear dynamic analytical requirement. Here, we extend the equivalent dynamic modeling to nonlinear forced vibration responses of the large NBT civil engineering structure with two pinned ends. We introduce the geometric nonlinearity into the equivalent dynamic model using the von Karman nonlinear strain-displacement relationship to imitate the nonlinear behaviors of the beamlike truss. On the basis of the Hamilton principle, the fourth-order governing partial differential equations of motion of the ENBM are obtained and solved utilizing the Galerkin method. It is shown that the ENBM accurately captures the nonlinear dynamic response of the beamlike truss subjected to external load by using the first four order modes. In order to showcase the efficiency and accuracy of the ENBM, time histories, phase maps and fast Fourier transform frequency spectra are investigated for the NBT and the ENBM under different external excitation magnitudes and frequencies. Comparisons between results of the ENBM and those obtained from the finite element simulations of the NBT show good agreements and identify the periodic motions of them. Furthermore, the effect of the external loading and damping parameters on the frequency-response and force-response curves is discussed. In addition, computing time of the proposed ENBM are compared with that of the full-scale finite element model in ANSYS so as to highlight the significant less computational cost of the equivalent nonlinear dynamic modeling. Particularly, the proposed ENBM can achieve the nonlinear mechanism of the NBT in analytical method and design the low-order control law conveniently.

1. Introduction

Truss structures composed of structural elements can achieve high stiffness and strength while at the same time significantly reduce the weight of the overall assembly [1]. Examples of the truss structure are ubiquitous in the engineering structures, e.g. buildings, bridges or transmission towers. Unfortunately, high-fidelity physics-based numerical simulation often bears an extremely large computational cost and cannot be utilized conveniently in the vibration controller design of the system due to large-scale, nonlinear nature of many truss structures; see, for instance, [2-4]. In such scenarios, the engineering requirements to apply such truss systems also call for advanced reduced-order technique of models. To this date, a large amount of previous work has been devoted to the theoretical and computational equivalent modeling of the truss structures [5-7].

During the past decades, some literatures investigated the design and nonlinear dynamic behavior of the truss structures to reach better convergence and computational efficiency. Kan et al. [8] addressed the dynamic properties of the clustered tensegrity based on the framework of positional formulation FEM. Habibi and Bidmeshki [9] presented a dual approach for geometrically nonlinear finite element analysis of plane truss structures, and the convergence of the analysis and reducing the number of required repeated analyses can be guaranteed utilizing optimization techniques. A viscous dynamic relaxation method was developed by Zardi and Alamatian based on the transformed Gershgorin circles theory. They employed this algorithm to evaluate the geometrically nonlinear behaviors of the 2D and 3D truss and frame structures [10]. Shi and Salim [11] discussed the nonlinear responses of guyed towers under static and dynamic loads using the developed nonlinear finite element method, which is possible to capture the complete geometric nonlinear response with the assistance of iterative algorithms. In Refs. [8] and [11], the nonlinear finite element methods were used directly to investigate the dynamic characteristics of the truss structures. By contrast, our study focuses on analyzing the nonlinear responses of

* Corresponding author.

E-mail address: dqcao@hit.edu.cn (D. Cao).

the truss structure by constructing its equivalent model, which is convenient to law-order controller design and analytical solution of the nonlinear beamlike truss. Applying the concept of computational mechanics, the nonlinear dynamic analysis of space truss structures are carried out in Ref. [12]. Similarly, it is also proposed according to the finite element method. Thai and Kim [13] predicted the geometric nonlinear responses of truss structures using an updated Lagrangian formulation and adopted an incremental-iterative solution scheme to solve the nonlinear equations of motion. Shekastehband and Ayoubi [14] studied the nonlinear dynamic instability behaviors of the tensegrity trusses subjected to impulsive loads. Based on the finite element method, two geometrically rigid configurations were analyzed to assess the dynamic instability. The nonlinear oscillations and dynamic stability of an elasto-plastic pyramidal truss were studied by Santana et al. [15] by using the finite element program. According to the finite element method, Mohit et al. [16] developed a new iterative method for geometrically nonlinear analysis of the space truss. Sohrabi et al. [17] formulated the nonlinear time-dependent deformation models for the electro-active truss structures and implemented the models in three-dimensional truss FEM. Two types of truss configurations are considered including the platelike and beamlike configurations. Above all, FEM is the main strategy to solve the nonlinear dynamic problems of the truss structures. However, it will take a lot of CPU time with the increase of structural complexity and dimension of the system. The equivalent dynamic modeling methodology is a very useful strategy to substitute the original nonlinear system making use of the periodicity of the structures [18–20]. Simultaneously, the equivalent modeling technique is convenient in the vibration controller designs of the large truss structures [21,22].

For the beamlike structures taking into account prestress forces, Liu et al. [22] and Ferretti [23] established equivalent Timoshenko beam models employing the energy equivalence principle and the homogenization approach, respectively. The nonlinear characteristics are not addressed in their researches. In fact, the study on the equivalent dynamic modeling taking account of the nonlinearity is quite limited up to now. Piccardo et al. built an equivalent nonlinear one-dimensional beam model for the tower buildings via the homogenization process [24] and established a continuous Timoshenko three-dimensional linear beam model to investigate the static and dynamic behavior of the tower buildings [25]. Then, D'Annibale et al. [26] followed Piccardo's work, developed shear-shear-torsional beam model for the multi-story frame buildings considering the nonlinearity caused by the stretch of the columns and the static responses are discussed using the perturbation method. Based on the dynamic equilibrium, an equivalent micropolar beam model was established for the planar repetitive truss structure with flexible joints utilizing the micropolar continuum theory [27]. Combining with the existing continuum model, Cao et al. [28] proposed a continuum model for the planar beam-like truss with geometrical nonlinearity based on the co-rotational formulation. Luongo and Zulli [29] used a homogenous beam model coming from a homogenization process to address the free and forced dynamic behavior of a multi-story building. Stephen and Ghosh [30] employed the equivalent curved beam to imitate the repetitive pin-jointed structure by using a state variable transfer matrix technique. Using the homogenization theory, Martin and Salehian [31] constructed a continuum model for the nonperiodic string-harnessed structures. Zhang et al. [32] put forward the equivalent models of the non-jointed and jointed structures based on the matrices of stiffness and mass, and evaluated the dynamic influences of the joints on the structure. According to the equivalent model of the large flexible structure, the distributed cooperative control of the flexible structure was studied in Ref. [33], which performs one significant advantage of the equivalent modelling technology. Adopting a Bloch-Floquet-based homogenization approach, Casalotti et al. [34] derived homogenized equivalent properties of a 2D lattice of regular hexagons to optimize the structure. For the lattice truss core sandwich beams, the dynamic equivalent beam parameters are identified using a wave finite element method [35]. Khakalo and Niiranen [36] developed a

pair of two-scale plate models for three-dimensional cellular plate-like structures based on the homogenization theory. To generate training sets for hyper-reduction of geometrically nonlinear structural dynamics problems, a quadratic manifold method was introduced in [37,38] and the offline cost was reduced. The equivalent modeling technique also has become an active research area in the material field [39,40]. Pal et al. [41] developed a continuum model exploiting the non-convex strain energy function for hexagonal lattices composed of a set of masses connected by linear axial and angular springs, with nonlinearity arising solely from geometric effects. Nady et al. [42] constructed an effective micropolar continuum for the periodic lattices to evaluate the nonlinear mechanical responses of the auxetic structures by using the homogenization method. A homogenization method was developed to establish the continuum model for the chiral lattice based on the micropolar theory [43]. Similarly, homogenization methods were employed to characterize the mechanics of cellular materials [44,45]. Phlipot and Kochmann [46] extended the QC methodology to general periodic truss considering the nonlinear deformations. Based on the homogenization theory, geometric nonlinearity of the lattice structures were taken into account [47,48]. Different remarkably from the above literatures, emphasis in this study is placed on the equivalent nonlinear dynamic modeling method based on the equivalent linear modeling technique [22]. To the best knowledge of the authors, there is limited related investigation concerning the geometric nonlinearity of the beamlike truss subjected to external force within the equivalent dynamic modeling. Therefore, it is crucial to develop an equivalent nonlinear dynamic modeling method, which can guarantee the accuracy and convergence of the equivalent model with significant less computational cost than the original structure.

The nonlinear beamlike truss is equivalent to a nonlinear Timoshenko beam model in this paper. The nonlinear dynamic behavior of beams has received considerable attention in the literature. These studies are based on either classical continuum models or the nonclassical continuum theories. Ghayesh et al. [49,50] studied the nonlinear dynamics of microscale beam based on the strain gradient elasticity theory and the modified couple stress theory, respectively. Ansari et al. [51,52] dealt with the nonlinear vibration behavior of the functionally graded beam with von Karman geometric nonlinearity employing the Timoshenko beam theory. A geometrically imperfect microbeam was presented to investigate its nonlinear dynamics and the frequency-response curves were constructed for the system with different initial imperfections [53]. Asghari et al. [54] delineated a nonlinear size-dependent Timoshenko beam model using the nonclassical continuum theory which can capture the size effects and the free vibration of a hinged-hinged beam is presented analytically utilizing the multiple scales method. Based on the modified couple stress theory, Reddy and Arbind [55,56] developed a microstructure-dependent beam considering the geometric nonlinearity and investigated the influence of the parameter on static bending, vibration and buckling. Yan et al. [57] analyzed the nonlinear flexural dynamic behavior of a clamped Timoshenko beam made of functionally graded materials with an open edge crack under an axial parametric excitation. Free vibration of functionally graded carbon nanotube-reinforced composite beams taking account of the von Karman geometric nonlinearity was performed according to the Timoshenko beam theory [58].

Most of previous equivalent models for truss structures were developed only considering small deformations and rotations. The geometric nonlinearity effects need to be considered within the extreme length of truss structures, but extremely rare works exist in this field. In Ref. [3], Goncalves et al. derived the equivalent stiffness matrix and geometric stiffness matrix for the periodic sandwich structures based on the force and moment equivalent principles, which were different from the energy equivalent principle utilized in this paper. Another vital difference is that the equivalent mass matrix was not derived and only static deformation of the structures were studied in Ref. [3]. Employing the displacement equivalent criterion, McCallen and Romstad [6] deduced the strain

energy of the equivalent model using nonlinear strain-displacement relationships handled by introducing an updated Lagrangian coordinate system and established an inadequacy of pure Timoshenko beam in to imitate the behaviors of the lattices. Similar to [3], the equivalent mass matrix was not derived. The pin-jointed truss structure was presented to establish its continuum model in [28] where the co-rotational formulation and linear equivalent model were combined to develop an extended continuum model of the beamlike truss structures with geometrical nonlinearity.

An important issue for the nonlinear dynamic analysis of the beamlike truss is to establish an effective dynamic model with just a few degrees of freedom. Using the FEM is a way to solve the nonlinear dynamic responses for the beamlike truss. However, the nonlinear FE model with high DOF requires a significant amount of computing capacity. Moreover, it is very difficult to do the analytical investigation for the system by using the FE model. For the nonlinear beamlike truss, the work considering directly the nonlinearity in the equivalent modeling process is extremely rare and a challenging research task. Therefore, the most significant developments of this paper are the establishment of the ENBM by introducing the nonlinear strain-displacement relationship into the linear equivalent dynamic model. Also, we go one step further to check whether the proposed ENBM is valid by using the Galerkin solving method. On the other hand, the ENBM can significantly reduce the computing time for the nonlinear investigations compared to the full-scale FE model of the truss structure.

The novelties of this study are to: 1) establish an equivalent nonlinear dynamic model for the beamlike truss with geometric nonlinearity handled by introducing von Karman nonlinear strain-displacement relationship on the linear equivalent model; 2) demonstrate the accuracy and high efficiency in computing of our method by studying various dynamic responses of the proposed ENBM and the NBT subjected to different external excitations. In addition, differing from previous equivalent modeling studies, the proposed ENBM involving the von Karman nonlinear strain-displacement relationship is checked comprehensively (including time histories, phase maps and fast Fourier transform frequency spectrum) by comparing with nonlinear full-scale finite element model of the beamlike truss. Furthermore, the nonlinear dynamic characteristics of the ENBM with parameter variation are studied, which paves way for future nonlinear study of the NBT in analytical method.

The remainder of this contribution is organized as follows. **Section 2** establishes the ENBM of the beamlike truss with two pinned ends based on the von Karman nonlinear strain-displacement feature employing the energy equivalence principle and the Timoshenko beam theory. **Section 3** reports the solution method of the nonlinear equations for the ENBM using the Hamilton principle and the Galerkin approach. **Section 4** assesses the accuracy and effectiveness of the ENBM by comparing with those nonlinear responses of the beamlike truss calculated from the full-scale FEM. Then, **Section 5** studies the nonlinear dynamic behaviors of the ENBM including the frequency-response and force-response curves. The effect of the mode order selected, damping, frequency and magnitude of the external load is investigated. Meanwhile, the computational efficiency is investigated to prove the high performance of the ENBM. Finally, **Section 6** concludes this investigation.

2. Establishment of the ENBM

2.1. System description

As shown in Fig. 1(a), we consider nonlinear beamlike truss (NBT) composed of longerons, battens and diagonals, which is produced by 36 spatial repeating elements (see Fig. 1(c)) along the axial direction. The longerons and battens are beams, and the diagonals are links. To obtain a continuum model of the beamlike truss, we establish the discrete assembly of beamlike truss by an effective ENBM, see Fig. 1(b).

Table 1
Material and dimensional parameters of the nonlinear beamlike truss.

Component	Parameter	Value
Longeron	Length L_l (mm)	2740
	Outer diameter D_l (mm)	100
	Thickness t_l (mm)	1
	Modulus of elasticity E_l (GPa)	69
	Poisson ratio μ_l	0.33
	Mass density ρ_l (kg/m ³)	2700
Batten	Height H (mm)	2771.3
	Outer diameter D_b (mm)	50
	Thickness t_b (mm)	1
	Modulus of elasticity E_b (GPa)	370
	Poisson ratio μ_b	0.22
	Mass density ρ_b (kg/m ³)	3960
Diagonal	Length L_d (mm)	4212.8
	Diameter D_d (mm)	6
	Modulus of elasticity E_d (GPa)	88
	Mass density ρ_d (kg/m ³)	1600

For the sake of calculation, the Cartesian coordinate system is built at the center of the repeating element, as shown in Fig. 1(c) and Fig. 1(d).

As shown in Fig. 1(a), a representative numerical example is investigated with the aim to study the ENBM of the NBT. The total length of the beamlike truss is 98.64m. The longerons and battens are made of aluminum alloy, and the diagonal cables are made of carbon fiber. The detailed material and dimensional parameters of the members are summarized in Table 1. The above formulation is sufficiently general to work with any choice of boundary conditions for the beamlike truss. For our equivalent dynamic modeling method study, we will select the following simply supported boundary condition as the nonlinear source of the system.

Based on the equivalent modeling method proposed in Ref. [22], the equivalent stiffness and the inertia items of the equivalent beam model for the beamlike truss can be achieved as

$$\overline{EA} = \frac{C_{11}}{L}, \quad \overline{EI}_z = \frac{C_{22}}{L}, \quad \overline{EI}_y = \frac{C_{33}}{L}, \quad \overline{GJ} = \frac{C_{44}}{L}, \\ \overline{GA}_{xz} = \frac{C_{55}}{L}, \quad \overline{GA}_{xy} = \frac{C_{66}}{L}. \quad (1)$$

$$\overline{\rho A} = \frac{B_{11}}{L} = \frac{B_{22}}{L} = \frac{B_{33}}{L}, \quad \bar{J}_x = \frac{B_{44}}{L}, \quad \bar{J}_y = \frac{1}{L} \left(B_{55} - \frac{1}{12} \overline{\rho A} L^3 \right), \\ \bar{J}_z = \frac{1}{L} \left(B_{66} - \frac{1}{12} \overline{\rho A} L^3 \right). \quad (2)$$

where \overline{EA} denotes the equivalent extension stiffness; \overline{EI}_z and \overline{EI}_y denote the equivalent bending stiffness; \overline{GJ} denotes the equivalent torsion stiffness; \overline{GA}_{xz} and \overline{GA}_{xy} denote the shearing stiffness. $\overline{\rho A}$ is the mass per unit length; \bar{J}_x , \bar{J}_y and \bar{J}_z are the rotational inertia per unit length. L is the length of the repeating element. The expressions of strain and kinetic energy coefficients C_{ii} , B_{ii} ($i = 1, 2, \dots, 6$) have been provided in the Appendix A.

Next, following the boundary condition of the beamlike truss, we consider the ENBM with length L_t also as the simply supported beam model which is illustrated in Fig. 2. It can be seen from the Eq. (1), the axial stiffness, bending stiffness and shearing stiffness on the x-y plane are \overline{EA} , \overline{EI}_z and \overline{GA}_{xy} , respectively. At the same time, the coordinate system and loading acting on the ENBM are also displayed in Fig. 2. A distributed transverse harmonic external force per unit length, $p(x)\sin(\Omega t)$, is exerted on the equivalent nonlinear beam model in the y direction. It should be reminded that the 2-dimensional ENBM is presented in this paper since the two directional bending vibrations are identical and uncoupled for the NBT. The x and y denote the axial and transverse components of the Cartesian coordinate, respectively. The displacements in the x and y directions (i.e. the longitudinal and trans-

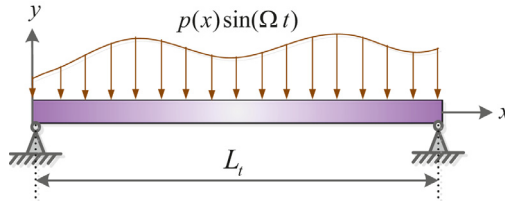
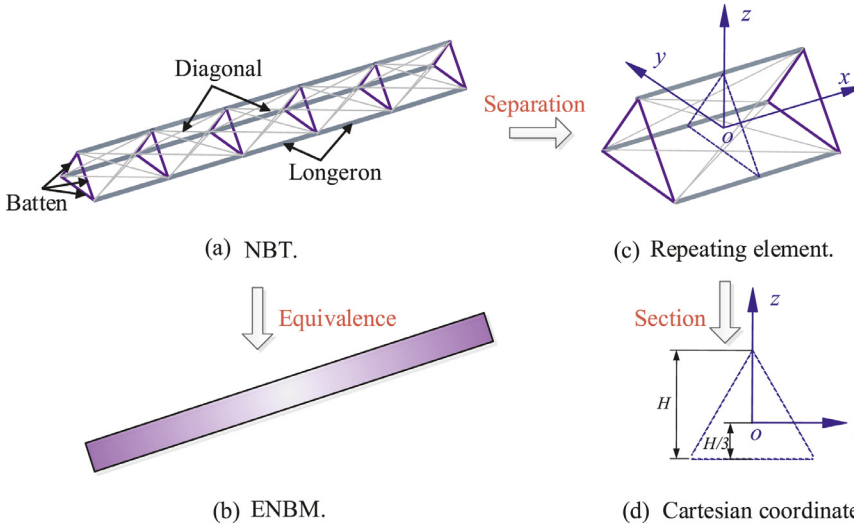


Fig. 2. Schematic representation of the equivalent nonlinear beam model (ENBM) with two pined ends subjected to a transverse distributed harmonic excitation force.

verse displacements) are denoted by $u_x(x, t)$ and $u_y(x, t)$, respectively; $\theta_z(x, t)$ is the rotation due to bending and shear angle.

According to the equivalent parameters of the ENBM in Eqs. (1) and (2), we will derive and solve the nonlinear dynamic responses for the ENBM of the nonlinear beamlike truss.

2.2. Nonlinear governing equations

The above ENBM is implemented using the Timoshenko beam theory. To this end, the source of the geometric nonlinearity for the ENBM is generated by the mid-plane stretching, for the simply supported boundary condition. In what follows, the nonlinear strain-displacement relations of the ENBM, associated with zero initial stresses, are evaluated by the von Karman relation as [59]

$$\varepsilon_x = \frac{\partial u_x}{\partial x} + \frac{1}{2} \left(\frac{\partial u_y}{\partial x} \right)^2, \quad \gamma_{xy} = \frac{\partial u_y}{\partial x} - \theta_z, \quad \kappa_y = \frac{\partial^2 u_y}{\partial x^2}. \quad (3)$$

in which ε_x , γ_{xy} and κ_y are the mid-plane extensional strain, shear strain and curvature of the ENBM, respectively.

Note that, the stiffness and inertia items of the ENBM have been achieved in Eqs. (1) and (2). To obtain the governing equations, the ENBM strain energy U due to extension, bending and shearing deformations stored energy in the system, and the kinetic energy T of the ENBM are calculated as follows

$$U = \frac{1}{2} \int_0^{L_t} \left[\overline{EA} \left(\frac{\partial u_x}{\partial x} + \frac{1}{2} \left(\frac{\partial u_y}{\partial x} \right)^2 \right)^2 + \overline{EI}_z \left(\frac{\partial \theta_z}{\partial x} \right)^2 + \overline{GA}_{xy} \left(\frac{\partial u_y}{\partial x} - \theta_z \right)^2 \right] dx \quad (4)$$

$$T = \frac{1}{2} \int_0^{L_t} \left[\overline{\rho A} \left(\frac{\partial u_x}{\partial t} \right)^2 + \overline{\rho A} \left(\frac{\partial u_y}{\partial t} \right)^2 + \overline{J_z} \left(\frac{\partial \theta_z}{\partial t} \right)^2 \right] dx \quad (5)$$

Fig. 1. Schematic view of (a) nonlinear beamlike truss composed of 36 spatial repeating elements, (b) equivalent nonlinear beam model used for imitating the nonlinear dynamic responses of the NBT, (c) separated repeating element and (d) Cartesian coordinate attached to the mid-cross section to establish the ENBM.

Subsequently, the expression for the virtual strain energy in the ENBM is given by

$$\begin{aligned} \int_{t_1}^{t_2} \delta U dt &= \int_{t_1}^{t_2} \left(- \int_0^{L_t} \left\{ \overline{GA}_{xy} [u''_y - \theta'_z] \delta u_y \right. \right. \\ &\quad \left. \left. + \overline{EA} \left[3/2 u'_y u''_y + u'_x u''_y + u''_x u'_y \right] \delta u_y \right. \right. \\ &\quad \left. \left. + \overline{EA} [u''_x + u'_y u''_y] \delta u_x + \left[\overline{EI}_z \theta''_z - \overline{GA}_{xy} \theta_z + \overline{GA}_{xy} u'_y \right] \delta \theta_z \right\} dx \right. \\ &\quad \left. + \overline{EA} [2u'_x + u'_y u''_y] \delta u_x \Big|_0^{L_t} + \overline{EA} \left[1/2 u'_y u''_y + u'_x u'_y \right] \delta u_y \Big|_0^{L_t} \right. \\ &\quad \left. + \overline{GA}_{xy} [u'_y - \theta_z] \delta u_y \Big|_0^{L_t} + \overline{EI}_z \theta'_z \delta \theta_z \Big|_0^{L_t} \right) dt \end{aligned} \quad (6)$$

The virtual kinetic energy is formulated as:

$$\int_{t_1}^{t_2} \delta T dt = \int_{t_1}^{t_2} \left(\int_0^{L_t} \left\{ -\overline{\rho A} \ddot{u}_x \delta u_x - \overline{\rho A} \ddot{u}_y \delta u_y - \overline{J_z} \ddot{\theta}_z \delta \theta_z \right\} dx \right) dt \quad (7)$$

Furthermore, the variations of the work done by the distributed harmonic excitation force δW_F and the viscous damping δW_D can be written as

$$\begin{aligned} \delta W_F &= \int_0^{L_t} p \delta u_y dx + N_1 \delta u_x(0, t) + N_2 \delta u_x(L_t, t) + Q_1 \delta u_y(0, t) \\ &\quad + Q_2 \delta u_y(L_t, t) + M_1 \delta \theta_z(0, t) + M_2 \delta \theta_z(L_t, t) \end{aligned} \quad (8)$$

$$\delta W_D = -c_d \int_0^{L_t} \left(\frac{\partial u_y}{\partial t} \delta u_y \right) dx - c_r \int_0^{L_t} \left(\frac{\partial \theta_z}{\partial t} \delta \theta_z \right) dx \quad (9)$$

where the axial forces N_1 and N_2 , moments M_1 and M_2 , shear forces Q_1 and Q_2 are the loads applied at the end boundaries of the ENBM as shown in Fig. 3. p is the external distributed loading. c_d and c_r stand for the viscous damping coefficients for the transverse displacement and rotation, respectively.

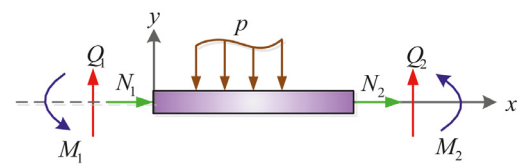


Fig. 3. External forces acting on the equivalent nonlinear beam model are presented to derive the nonlinear governing equations and boundary conditions.

Substituting Eqs. (6)-(9) into the Hamilton principle, can result in the form:

$$\int_{t_1}^{t_2} (\delta T - \delta U + \delta W_F + \delta W_D) dt = 0 \quad (10)$$

and there are $\delta u_x(x, t_1) = \delta u_x(x, t_2) = 0$, $\delta u_y(x, t_1) = \delta u_y(x, t_2) = 0$ and $\delta \theta_z(x, t_1) = \delta \theta_z(x, t_2) = 0$.

Thus, we can obtain the following nonlinear partial differential equations governing the longitudinal, transverse and rotational motions of the ENBM:

$$\overline{EA} \frac{\partial^2 u_x}{\partial x^2} + \overline{EA} \frac{\partial u_y}{\partial x} \frac{\partial^2 u_y}{\partial x^2} - \rho A \frac{\partial^2 u_x}{\partial t^2} = 0 \quad (11)$$

$$\begin{aligned} & \overline{EA} \left(\frac{3}{2} \left(\frac{\partial u_y}{\partial x} \right)^2 \frac{\partial^2 u_y}{\partial x^2} + \frac{\partial u_y}{\partial x} \frac{\partial^2 u_x}{\partial x^2} + \frac{\partial u_x}{\partial x} \frac{\partial^2 u_y}{\partial x^2} \right) + \overline{GA}_{xy} \left(\frac{\partial^2 u_y}{\partial x^2} - \frac{\partial \theta_z}{\partial x} \right) \\ & - \rho A \frac{\partial^2 u_y}{\partial t^2} - c_d \frac{\partial u_y}{\partial t} + p(x) \sin(\Omega t) = 0 \end{aligned} \quad (12)$$

$$\overline{EI}_z \frac{\partial^2 \theta_z}{\partial x^2} - \overline{GA}_{xy} \theta_z + \overline{GA}_{xy} \frac{\partial u_y}{\partial x} - \overline{J}_z \frac{\partial^2 \theta_z}{\partial t^2} - c_r \frac{\partial \theta_z}{\partial t} = 0 \quad (13)$$

with the following boundary conditions for simply supported beam with immovable ends

$$u_x|_{x=0} = u_x|_{x=L_t} = 0, \quad u_y|_{x=0} = u_y|_{x=L_t} = 0, \quad \frac{\partial \theta_z}{\partial x}|_{x=0} = \frac{\partial \theta_z}{\partial x}|_{x=L_t} = 0. \quad (14)$$

3. Solution method of nonlinear equations

In this section, the basic assumption is introduced and solution method is presented for the nonlinear equations of motion. Obviously, Eqs. (11)-(13) are coupled and nonlinearity is caused by the mid-plane stretching due to the two immovable ends. In general, the longitudinal inertia is small compared with both the transverse inertia and the rotary inertia. In this case, ignoring the longitudinal inertia term $\rho A \partial^2 u_x / \partial t^2$ in Eq. (11) and on the basis of boundary conditions $u_x|_{x=0} = u_x|_{x=L_t} = 0$, we arrive at

$$\overline{EA} \left(\frac{\partial u_x}{\partial x} + \frac{1}{2} \left(\frac{\partial u_y}{\partial x} \right)^2 \right) = \frac{\overline{EA}}{2L_t} \int_0^{L_t} \left(\frac{\partial u_y}{\partial x} \right)^2 dx \quad (15)$$

As expected, inserting Eq. (15) into Eq. (12) can eliminate the parameter u_x and Eq. (12) can be rewritten as

$$\rho A \frac{\partial^2 u_y}{\partial t^2} - \overline{GA}_{xy} \frac{\partial^2 u_y}{\partial x^2} + \overline{GA}_{xy} \frac{\partial \theta_z}{\partial x} - N_x \frac{\partial^2 u_y}{\partial x^2} + c_d \frac{\partial u_y}{\partial t} - p(x) \sin(\Omega t) = 0 \quad (16)$$

in which

$$N_x = N_0 + \frac{\overline{EA}}{2L_t} \int_0^{L_t} \left(\frac{\partial u_y}{\partial x} \right)^2 dx \quad (17)$$

where N_0 is the initial axial tensile force.

In order to achieve the governing equation only includes the variation u_y , combining Eqs. (13) and (16) gives the following equation that governs the transverse deflections u_y

$$\begin{aligned} & \overline{EI}_z \frac{\partial^4 u_y}{\partial x^4} + \rho A \frac{\partial^2 u_y}{\partial t^2} - \left(\overline{J}_z + \frac{\rho A \cdot \overline{EI}_z}{\overline{GA}_{xy}} \right) \frac{\partial^4 u_y}{\partial x^2 \partial t^2} + \frac{\rho A \cdot \overline{J}_z}{\overline{GA}_{xy}} \frac{\partial^4 u_y}{\partial t^4} \\ & + N_x \left(\frac{\overline{EI}_z}{\overline{GA}_{xy}} \frac{\partial^4 u_y}{\partial x^4} - \frac{\overline{J}_z}{\overline{GA}_{xy}} \frac{\partial^4 u_y}{\partial x^2 \partial t^2} - \frac{\partial^2 u_y}{\partial x^2} \right) \\ & + p(x) \sin(\Omega t) \left(\frac{\overline{J}_z \cdot \Omega^2}{\overline{GA}_{xy}} - 1 \right) \end{aligned}$$

$$\begin{aligned} & + c_d \left(\frac{\partial u_y}{\partial t} + \frac{\overline{J}_z}{\overline{GA}_{xy}} \frac{\partial^3 u_y}{\partial t^3} - \frac{\overline{EI}_z}{\overline{GA}_{xy}} \frac{\partial^3 u_y}{\partial x^2 \partial t} \right) + \frac{c_d c_r}{\overline{GA}_{xy}} \frac{\partial^2 u_y}{\partial t^2} \\ & + c_r \left(\frac{\rho A}{\overline{GA}_{xy}} \frac{\partial^3 u_y}{\partial t^3} - \frac{p(x) \cdot \Omega}{\overline{GA}_{xy}} \cos(\Omega t) - \left(1 + \frac{N_x}{\overline{GA}_{xy}} \right) \frac{\partial^3 u_y}{\partial x^2 \partial t} \right) = 0 \end{aligned} \quad (18)$$

Let $p(x) = p_0$ in the following sections. From a solution perspective, it is convenient to introduce several dimensionless parameters, as

$$\begin{aligned} x^* &= \frac{x}{L_t}, \quad u_y^* = \frac{u_y}{L_t}, \quad c_d^* = \frac{c_d L_t^4}{\overline{EI}_z} \sqrt{\frac{\overline{EI}_z}{\rho A \cdot L_t^4}}, \quad c_r^* = \frac{c_r \cdot \overline{EA} \cdot L_t^4}{(\overline{EI}_z)^2} \sqrt{\frac{\overline{EI}_z}{\rho A \cdot L_t^4}}, \\ t^* &= t \sqrt{\frac{\overline{EI}_z}{\rho A \cdot L_t^4}}, \quad \Omega^* = \Omega \sqrt{\frac{\rho A \cdot L_t^4}{\overline{EI}_z}}, \quad p_0^* = \frac{p_0 L_t^3}{\overline{EI}_z}. \end{aligned} \quad (19)$$

Substituting above parameters into Eq. (18) and dropping the asterisk notation for brevity results in the following dimensionless nonlinear partial differential equations of motion for the transverse:

$$\begin{aligned} & \frac{\partial^4 u_y}{\partial x^4} + \frac{\partial^2 u_y}{\partial t^2} - \frac{1}{L_t^2} \left(\frac{\overline{EI}_z}{\overline{GA}_{xy}} + \frac{\overline{J}_z}{\rho A} \right) \frac{\partial^4 u_y}{\partial x^2 \partial t^2} + \frac{\overline{EI}_z \cdot \overline{J}_z}{L_t^4 \cdot \overline{GA}_{xy} \cdot \rho A} \frac{\partial^4 u_y}{\partial t^4} \\ & - N_x \left[\frac{\partial^2 u_y}{\partial x^2} - \frac{\overline{EI}_z}{L_t^2 \cdot \overline{GA}_{xy}} \frac{\partial^4 u_y}{\partial x^4} + \frac{\overline{J}_z \cdot \overline{EI}_z}{L_t^4 \cdot \overline{GA}_{xy} \cdot \rho A} \frac{\partial^4 u_y}{\partial x^2 \partial t^2} \right] \\ & + p_0 \sin(\Omega t) \left(\frac{\overline{EI}_z \cdot \overline{J}_z \cdot \Omega^2}{L_t^4 \cdot \rho A \cdot \overline{GA}_{xy}} - 1 \right) \\ & + c_d \left[\frac{\partial u_y}{\partial t} - \frac{\overline{EI}_z}{\overline{GA}_{xy} \cdot L_t^2} \frac{\partial^3 u_y}{\partial x^2 \partial t} + \frac{\overline{EI}_z \cdot \overline{J}_z}{L_t^4 \cdot \overline{GA}_{xy} \cdot \rho A} \frac{\partial^3 u_y}{\partial t^3} \right] \\ & + c_d c_r \frac{\overline{EI}_z^2}{L_t^4 \cdot \overline{GA}_{xy} \cdot \overline{EA}} \frac{\partial^2 u_y}{\partial t^2} \\ & + c_r \left[\frac{\overline{EI}_z^2}{L_t^4 \cdot \overline{GA}_{xy} \cdot \overline{EA}} \frac{\partial^3 u_y}{\partial t^3} - \frac{\overline{EI}_z^2 \cdot p_0 \cdot \Omega}{L_t^4 \cdot \overline{GA}_{xy} \cdot \overline{EA}} \cos(\Omega t) \right. \\ & \left. - \frac{\overline{EI}_z}{\overline{EA} \cdot L_t^2} \left[1 + \frac{N_x}{\overline{GA}_{xy}} \right] \frac{\partial^3 u_y}{\partial x^2 \partial t} \right] = 0 \end{aligned} \quad (20)$$

where

$$N_x = \frac{N_0 L_t^2}{\overline{EI}_z} + \frac{L_t^2 \cdot \overline{EA}}{2\overline{EI}_z} \int_0^1 \left(\frac{\partial u_y}{\partial x} \right)^2 dx \quad (21)$$

In the following, the Galerkin approach is employed to discretize and reduce Eq. (20) into a set of nonlinear ordinary differential equations with finite number of degrees of freedom. The eigenfunction for the transverse motion of a hinged-hinged linear beam is chosen as the appropriate basis functions for the transverse motion of the ENBM. For this reason, the eigenfunction $\phi_k(x)$ of a hinged-hinged linear beam are

$$\phi_k(x) = \sin(k\pi x) \quad k = 1, 2, 3 \dots \quad (22)$$

Therefore, the transverse displacement of the system is assumed as the following approximate series expansions:

$$u_y(x, t) = \sum_{k=1}^M \phi_k(x) q_k(t) \quad (23)$$

in which $\phi_k(x)$ is the k th eigenfunction for the transverse motion of a hinged-hinged linear beam and $q_k(t)$ is the corresponding generalized coordinate for the transverse motion.

Eq. (23) is substituted into (20) and the resultant equation is multiplied by the corresponding eigenfunction $\phi_i(x)$ and integrated from 0 to 1, which yields the following desired nonlinear ordinary differential

equations:

$$\begin{aligned} \alpha_1 \sum_{k=1}^M \left(\int_0^1 \phi_i \phi_k dx \right) q_k^{(4)} + \left[\sum_{k=1}^M \left(\int_0^1 \phi_i \phi_k dx \right) + \alpha_2 \sum_{k=1}^M \left(\int_0^1 \phi_i \phi''_k dx \right) \right] \ddot{q}_k & (24) \\ + \alpha_3 \sum_{k=1}^M \sum_{j=1}^M \left(\int_0^1 \phi_i \phi''_k \phi'^2_j dx \right) \ddot{q}_k q_j^2 + \alpha_4 \sum_{k=1}^M \sum_{j=1}^M \left(\int_0^1 \phi_i \phi''_k \phi'^2_j dx \right) q_k q_j^2 & (24) \\ + \alpha_5 \sum_{k=1}^M \sum_{j=1}^M \left(\int_0^1 \phi_i \phi_k^{(4)} \phi'^2_j dx \right) q_k q_j^2 + \sum_{k=1}^M \left(\int_0^1 \phi_i \phi_k^{(4)} dx \right) q_k \\ + \alpha_6 \sum_{k=1}^M \left(\int_0^1 \phi_i \phi_k dx \right) \dot{q}_k + \alpha_7 \sum_{k=1}^M \left(\int_0^1 \phi_i \phi''_k dx \right) \dot{q}_k + \alpha_8 \sum_{k=1}^M \left(\int_0^1 \phi_i \phi_k dx \right) q_k^{(3)} \\ + \alpha_9 \sum_{k=1}^M \left(\int_0^1 \phi_i \phi_k dx \right) \ddot{q}_k + \alpha_{10} \sum_{k=1}^M \sum_{j=1}^M \left(\int_0^1 \phi_i \phi''_k \phi'^2_j dx \right) \ddot{q}_k q_j^2 \\ + p_0 (\alpha_{11} \sin(\Omega t) + \alpha_{12} \cos(\Omega t)) \int_0^1 \phi_i dx = 0. & (24) \end{aligned}$$

where the dot and prime notations denote the differentiations with respect to the dimensionless time axial coordinate, respectively. Supercripts (4) and (3) represent the fourth and third derivations with respect to the dimensionless time axial coordinate, respectively. $i = 1, 2, \dots, M$. and $\alpha_n (n = 1, 2, \dots, 12)$ are the coefficients given as:

$$\begin{aligned} \alpha_1 &= \frac{\overline{EI_z} \cdot \overline{J_z}}{L_t^4 \cdot \overline{GA_{xy}} \cdot \overline{\rho A}}, \quad \alpha_2 = -\frac{\overline{EI_z} \cdot \overline{\rho A} + \overline{GA_{xy}} \cdot \overline{J_z}}{\overline{GA_{xy}} \cdot \overline{\rho A} \cdot L_t^2}, \quad \alpha_3 = -\frac{\overline{EA} \cdot \overline{J_z}}{2L_t^2 \cdot \overline{GA_{xy}} \cdot \overline{\rho A}}, \\ \alpha_4 &= -\frac{\overline{EA} \cdot L_t^2}{2\overline{EI_z}}, \quad \alpha_5 = \frac{\overline{EA}}{\overline{GA_{xy}}}, \quad \alpha_6 = c_d, \quad \alpha_7 = -\frac{c_d \cdot \overline{EI_z}}{\overline{GA_{xy}} \cdot L_t^2} - \frac{c_r \cdot \overline{EI_z}}{\overline{EA} \cdot L_t^2}, \\ \alpha_8 &= \frac{c_d \cdot \overline{EI_z} \cdot \overline{J_z}}{\overline{\rho A} \cdot \overline{GA_{xy}} \cdot L_t^4} + \frac{c_r \cdot \overline{EI_z}^2}{\overline{EA} \cdot \overline{GA_{xy}} \cdot L_t^4}, \quad \alpha_9 = \frac{c_d \cdot c_r \cdot \overline{EI_z}^2}{\overline{EA} \cdot \overline{GA_{xy}} \cdot L_t^4}, \\ \alpha_{10} &= -\frac{c_r}{2\overline{GA_{xy}}}, \quad \alpha_{11} = \frac{\overline{EI_z} \cdot \overline{J_z} \cdot \Omega^2}{\overline{\rho A} \cdot \overline{GA_{xy}} \cdot L_t^4} - 1, \quad \alpha_{12} = -c_r \frac{\overline{EI_z}^2 \cdot \Omega}{\overline{EA} \cdot \overline{GA_{xy}} \cdot L_t^4}. & (25) \end{aligned}$$

The developed method above can be used to simulate the forced vibration responses with harmonic loadings of the ENBM by numerical method. Although Zhang et al. [60] established the continuous model of a circular mesh antenna and the nonlinear dynamic response was carried out for the equivalent circular cylindrical short shell model. It ought to be pointed out that comparison with those results of the circular mesh antenna was not conducted so that the validity of the equivalent model can be checked to some extent, and the equivalent model also cannot imitate the nonlinear behaviors of the antenna. In this study, the numerical results, including natural frequencies, time histories, phase maps and fast Fourier transform frequency spectra are exhibited to a good accuracy and effectiveness of the ENBM by comparing with those results from ANSYS simulation of full-scale beamlike truss finite element model. Moreover, the effects of the variational parameters on the nonlinear behaviors are analyzed reasonably.

4. Comparative responses analysis of ENBM and NBT

In order to verify the validity of the ENBM, a numerical result comparison between the ENBM and the full-scale finite element model of the nonlinear beamlike truss (NBT) is investigated. In addition, emphasis will be placed on the first four order modes of the ENBM, to display the nonlinear dynamics of the ENBM. It should be noted that as a result of symmetrical configuration of two systems (NBT and ENBM) and the external forces, only the symmetric modes affect the dynamic response of the system.

We demonstrate the performance of the theory and numerical implementation described above by simulating the nonlinear dynamics of the beamlike truss using both the proposed equivalent modeling method and a discrete truss finite element calculation for comparison. Substituting Eq. (22) into (24), the 4 fourth-order obtained nonlinear ordinary differential equations can be solved applying numerical method. Meanwhile, we compute the nonlinear behaviors of the beamlike truss applying full-scale FEM in ANSYS. Note that the non-dimensional numerical

Table 2

Comparisons of natural frequencies between the LBT and ELBM.

Frequency order	LBT (Hz)	ELBM (Hz)	Error (%)
1	0.7427	0.7475	0.6463
2	2.8112	2.8209	0.3450
3	5.8365	5.8353	0.0206
4	9.4351	9.4050	0.3190

results obtained are substituted into Eq. (19) to get the dimensional results which are used in the discussions in the following. In Table 2, the evaluated first four natural frequencies of the equivalent linear beam model (ELBM) are presented as comparisons with those obtained from the full-scale finite element model of the linear beamlike truss (LBT). According to Table 2, it can be observed that the results generated through the proposed ELBM are in good agreement with ones for beamlike truss. The maximum error of natural frequencies for the first four orders is only 0.6463%.

For the undamped case, numerical simulations have been carried out by the nonlinear system (24) and the nonlinear beamlike truss system in ANSYS by varying the external force magnitude $p_0 = 50\text{N/m}$, 100N/m and frequency $\Omega = 0.5\text{Hz}$, 1Hz to compare the nonlinear response of the proposed ENBM with those of the NBT. The nonlinear responses of the undamped ENBM and NBT within ten seconds are studied as shown in Fig. 4-5. In Fig. 4 is shown the time histories at the midpoint positions of the ENBM and NBT for two special values of excitation frequency under $p_0 = 50\text{N/m}$. The broken lines in the figure are the results of the NBT and the full lines are calculated by the ENBM. It can be immediately seen that the two sets of data are in good agreement. To fully investigate the influence of the external force and the excitation frequency on the accuracy of the ENBM, the time histories under $p_0 = 100\text{N/m}$ is adopted to perform the validity study, as shown in Fig. 5. As is evident, it can be found that the results obtained by the present equivalent modeling method are agree excellently with those computed by the full-scale FEM of the beamlike truss. This can verify the proposed ENBM is accurate. Inspecting these plots, the numerical results can reveal that the amplitudes of the nonlinear response grow with the increase of the external force. The first linear natural frequency of the beamlike truss has been found to be $\omega_1 = 0.7427\text{Hz}$ as illustrated in Table 2. In particular, the nonlinear responses of the two systems (NBT and ENBM) are larger around the first linear natural frequency than those far away from ω_1 within certain limits.

Moreover, the vibration form of displacements time histories covering the whole systems is explored for external loading $p_0 = 50\text{N/m}$. The displacement time histories for the ENBM and the NBT with $\Omega = 0.5\text{Hz}$ and $\Omega = 1\text{Hz}$ are displayed in Fig. 6 and Fig. 7, respectively. It is clear to see that the displacements time histories of the two systems have a similar trend and the curves are substantially identical. Once again, the proposed ENBM can imitate the nonlinear responses of the NBT effectively.

For the purpose of comparison, Fig. 8(a)-(d) summarize the steady responses, phase maps and fast Fourier transform frequency spectra at the midpoint positions of the ENBM and the NBT with different external excitation frequencies when $p_0 = 25\text{N/m}$, $c_d = 1.19\text{N} \cdot \text{s}/\text{m}^2$, $c_r = 2.15\text{N} \cdot \text{s}$. As the Fig. 8 shown, the ENBM and NBT responses in steady-state phase are in good agreement under $\Omega = 0.5\text{Hz}$, 1Hz , 1.5Hz , 3Hz and the nonlinear responses of the beamlike truss are sufficiently well captured by the ENBM. Simultaneously, it is clear that the phase portraits and the frequency spectra of the ENBM match well with those results of the NBT. We find that the two systems are periodic motion from the phase portraits. It can also be observed from Fig. 8 that a dominant frequency can be found in frequency spectrum curves. The two systems are forced vibration and the vibration frequencies are the same as the external excitation frequencies. Away from the external excitation frequency, the vibration amplitudes of the two systems become small.

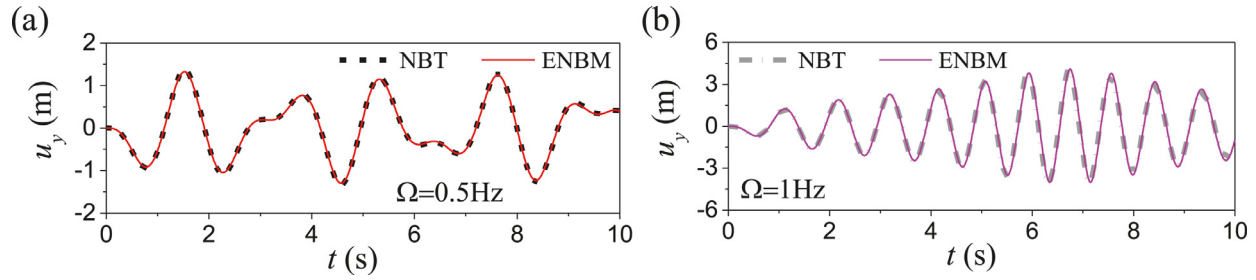


Fig. 4. Time histories at the midpoints of the ENBM and NBT under different external excitation frequencies Ω : (a) $\Omega=0.5\text{Hz}$ and (b) $\Omega=1\text{Hz}$. To validate the proposed ENBM, the time history curves within ten seconds are presented by full lines for ENBM and broken lines for NBT. The external force magnitude is set as $p_0 = 50\text{N/m}$, $c_d = c_r = 0$.

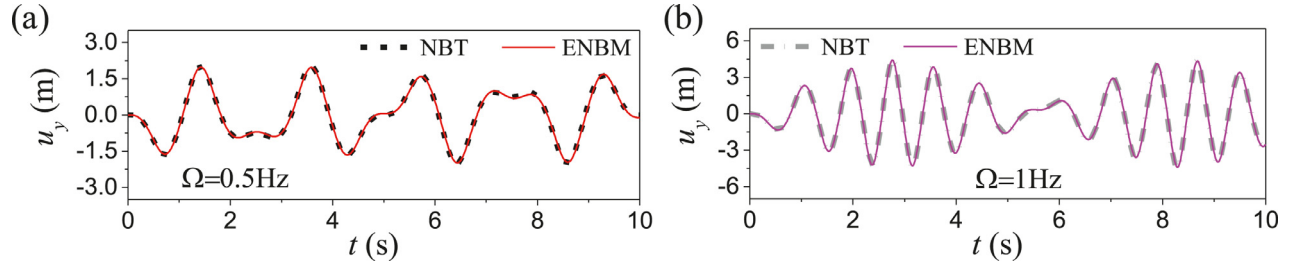


Fig. 5. Time histories at the midpoints of the ENBM and NBT under different external excitation frequencies Ω : (a) $\Omega=0.5\text{Hz}$ and (b) $\Omega=1\text{Hz}$. To validate the proposed ENBM, the time history curves within ten seconds are presented by full lines for ENBM and broken lines for NBT. The external force magnitude is set as $p_0 = 100\text{N/m}$, $c_d = c_r = 0$.

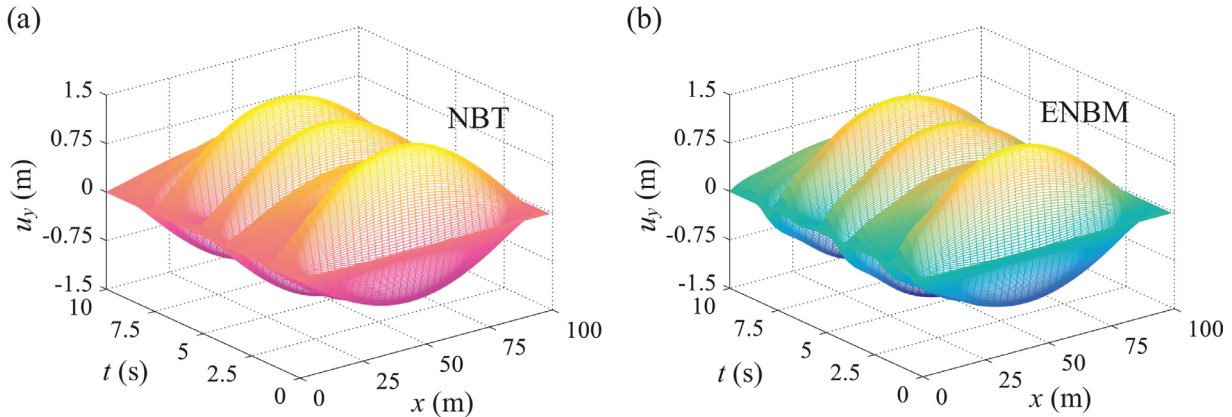


Fig. 6. Displacements time histories at the midpoints of (a) the nonlinear beamlike truss and (b) the equivalent nonlinear beam model to detect the consistency, for the parameter values $p_0 = 50\text{N/m}$, $\Omega=0.5\text{Hz}$ and $c_d = c_r = 0$.

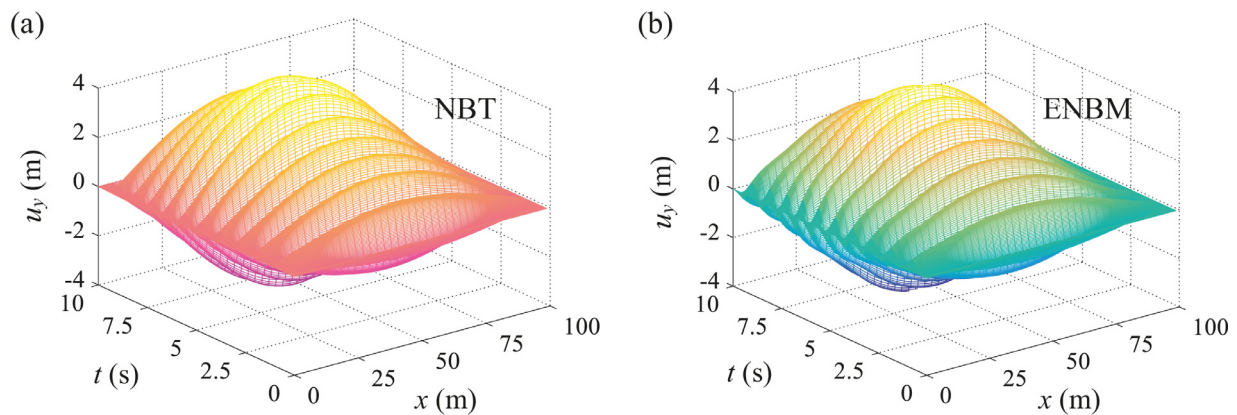


Fig. 7. Displacements time histories at the midpoints of (a) the nonlinear beamlike truss and (b) the equivalent nonlinear beam model to detect the consistency, for the parameter values $p_0 = 50\text{N/m}$, $\Omega=1\text{Hz}$ and $c_d = c_r = 0$.

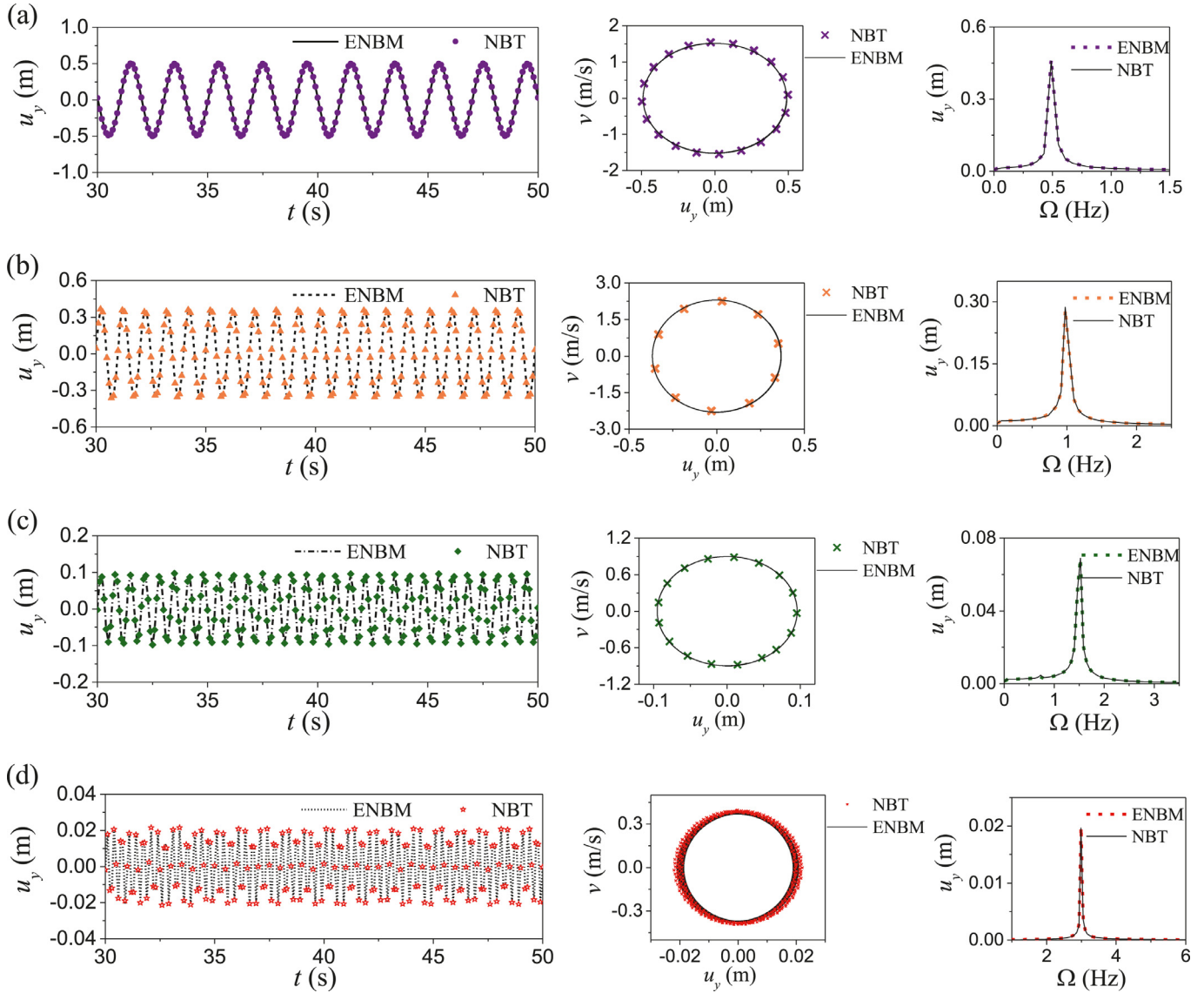


Fig. 8. Comparisons of steady-state responses for the proposed equivalent nonlinear beam model and the nonlinear beamlike truss to check the validity under different external excitation frequencies (a) $\Omega = 0.5\text{Hz}$, (b) $\Omega = 1\text{Hz}$, (c) $\Omega = 1.5\text{Hz}$ and (d) $\Omega = 3\text{Hz}$, for the parameter values $p_0 = 25\text{N/m}$, $c_d = 1.19\text{N}\cdot\text{s}/\text{m}^2$ and $c_r = 2.15\text{N}\cdot\text{s}$.

Similarly, Fig. 9 is presented to explore the effects of force magnitude on the accuracy of the ENBM and nonlinear responses of the two systems when $p_0 = 50\text{N/m}$. As depicted, the time histories, phase maps and frequency spectra are also in good agreements between the ENBM and the NBT. Hence, it can be concluded that the nonlinear beamlike truss is efficiently modeled by the proposed ENBM through the comparisons of numerical result. And, the nonlinear behaviors of the beamlike truss can be captured well by the ENBM.

To validate the power of the proposed ENBM in predicting the strong nonlinear response of the NBT, a numerical example of highly nonlinear effect under large external force $p_0 = 500\text{N/m}$ is performed next. The comparisons of the time histories, phase maps and frequency spectra calculated from ENBM and NBT are provided in Fig. 10 with $p_0 = 500\text{N/m}$. Fig. 10 shows that the nonlinear responses of the proposed ENBM match well with those of the NBT in this case. The results demonstrate that the ENBM can capture excellently the nonlinear dynamic response of the NBT even through the large external force subjects to the truss. In addition, it can be found from Fig. 10(a) and Fig. 10(b) that for the cases of $\Omega = 0.5\text{Hz}$ and $\Omega = 1\text{Hz}$, the responses include more than one frequency components due to the nonlinear coupling terms in the ENBM and NBT.

Here, our main focus is on the computational efficiency of the proposed modeling method and full-scale FEM. The time consumption of the nonlinear response in 50s for the ENBM and full-scale beamlike truss is recorded using a PC with a 3.30 GHz CPU and 8GB of RAM. Computational time of the ENBM and the NBT is 24.2s and 17025.15s, respectively, and the time ratio between the ENBM and the NBT is approximately 1/704. It becomes immediately clear that establishment of the ENBM and solution method for the nonlinear governing equations can save huge computer resource. Furthermore, unlike the controller design and analytical solution difficulties existed in the FEM, the ENBM can avoid these defects available. Therefore, the proposed ENBM can exhibit an excellent performance for the nonlinear analysis, even for the optimization of the beamlike truss.

5. Nonlinear dynamic analysis of ENBM

In this subsection, the nonlinear dynamic study for a finite number of modes of the ENBM is exhibited. Moreover, the effect of the number of selected modes, the distributed harmonic excitation forces and damping parameters on the frequency-response and force-response curves of the

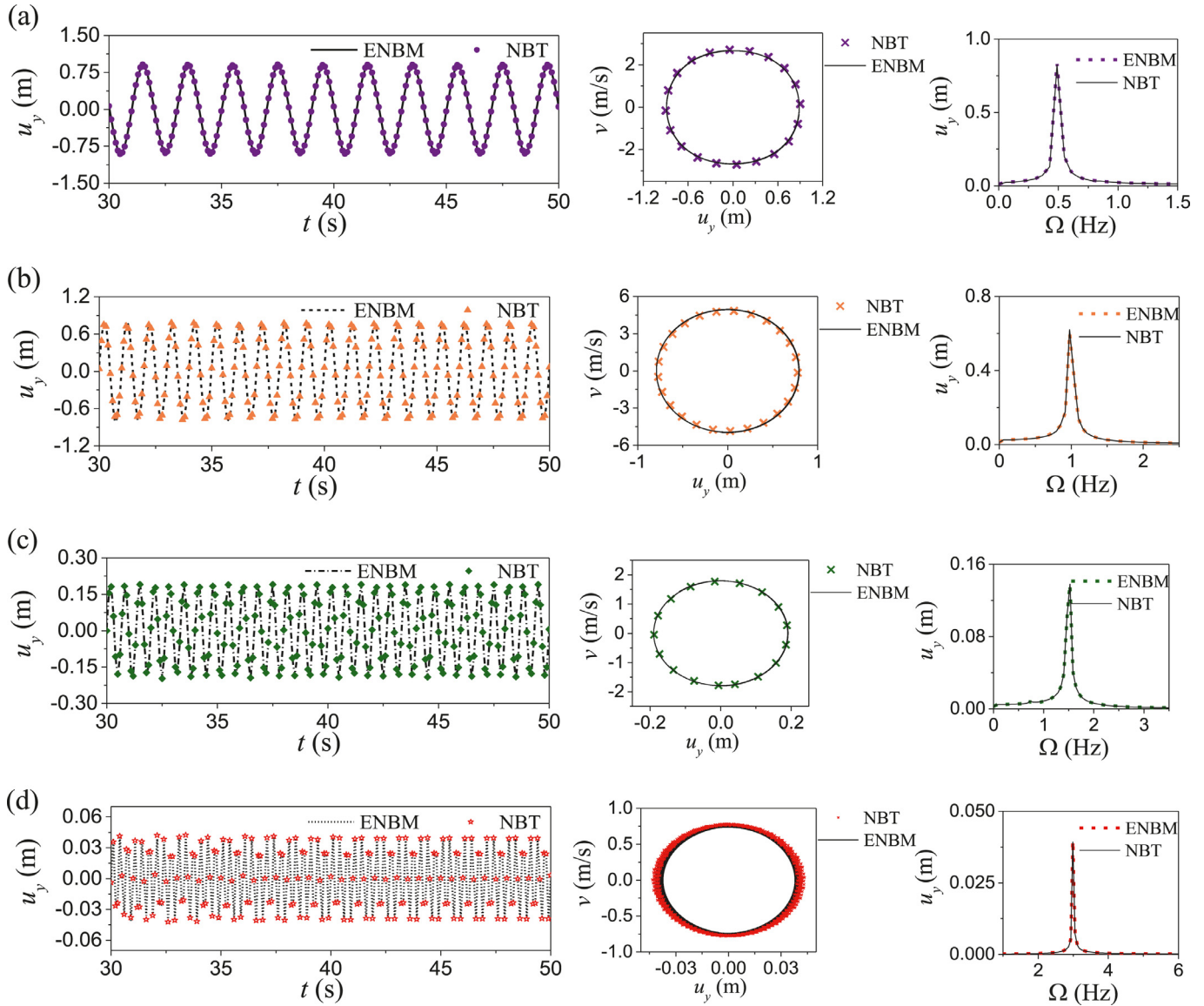


Fig. 9. Comparisons of steady-state responses for the proposed equivalent nonlinear beam model and the nonlinear beamlike truss to check the validity under different external excitation frequencies (a) $\Omega = 0.5\text{Hz}$, (b) $\Omega = 1\text{Hz}$, (c) $\Omega = 1.5\text{Hz}$ and (d) $\Omega = 3\text{Hz}$, for the parameter values $p_0 = 50\text{N/m}$, $c_d = 1.19\text{N} \cdot \text{s}/\text{m}^2$ and $c_r = 2.15\text{N} \cdot \text{s}$.

ENBM is analyzed so that to some extent these results can stand for the nonlinear characteristics of the NBT.

Firstly, in the following we investigate the frequency-response and force-response curves of the ENBM by selecting the first fourth modes, which are constructed as the frequency of the external excitation is varied around the first linear natural frequency $\omega_1 = 0.75\text{Hz}$ of the transverse motion. The transverse displacement is computed via Eq. (23), representing the absolute maximum displacement at the middle point of the ENBM with two pinned ends. In Fig. 11, the frequency-response curves exhibit hardening behavior as same to the case of a general Timoshenko beam which is a hardening type. Actually, hysteresis behavior is visible from the frequency-response curve of the system where the displacement amplitude of the ENBM depends not only on the current excitation frequency, but also on the history of past excitation frequencies. Thus, it is observed that the system follows two different paths for the cases when the excitation frequency Ω is increased from point E or decreased from point F. As seen in Fig. 11(a), there are two limit point bifurcations present: the first one is responsible for an upward jump from the high amplitude motion to the lower amplitude one, and

second one for a reverse scenario. The first and second limit points correspond, respectively, to $\Omega \approx 0.155\text{Hz}$ (point A) and $\Omega \approx 0.9\text{Hz}$ (point C) for the external excitation force $p_0 = 25\text{N/m}$. With the increase of p_0 , the vibration amplitude increase from 5.4m to 8.0m, and the first and second limit points become $\Omega \approx 2.15\text{Hz}$ (point A) and $\Omega \approx 1\text{Hz}$ (point C), respectively, as shown in Fig. 11(b). When the excitation frequency is increased from $\Omega=0$, it is found that the response amplitude is increased gradually. It should be mentioned that at each of points A and C, the system becomes unstable resulting in the occurrence of a bifurcation and hence a jump to either a lower amplitude (point B) or higher amplitude (point D) stable branch. Fig. 11 shows the point A is associated with the nonlinear resonance of the system where it reaches maximum amplitude.

It is then of interest to explore the effect of the viscous damping coefficients c_d and c_r on the dynamical responses of the ENBM. Typical results are shown in Fig. 12 for $p_0 = 25\text{N/m}$ and $p_0 = 50\text{N/m}$. Inspecting these plots, we note that the frequency-response curves for $c_d = c_r = 0.3$, 0.5 and 0.7 have a similar trend when the excitation frequency is successively varied (either increased or decreased). Nevertheless, the

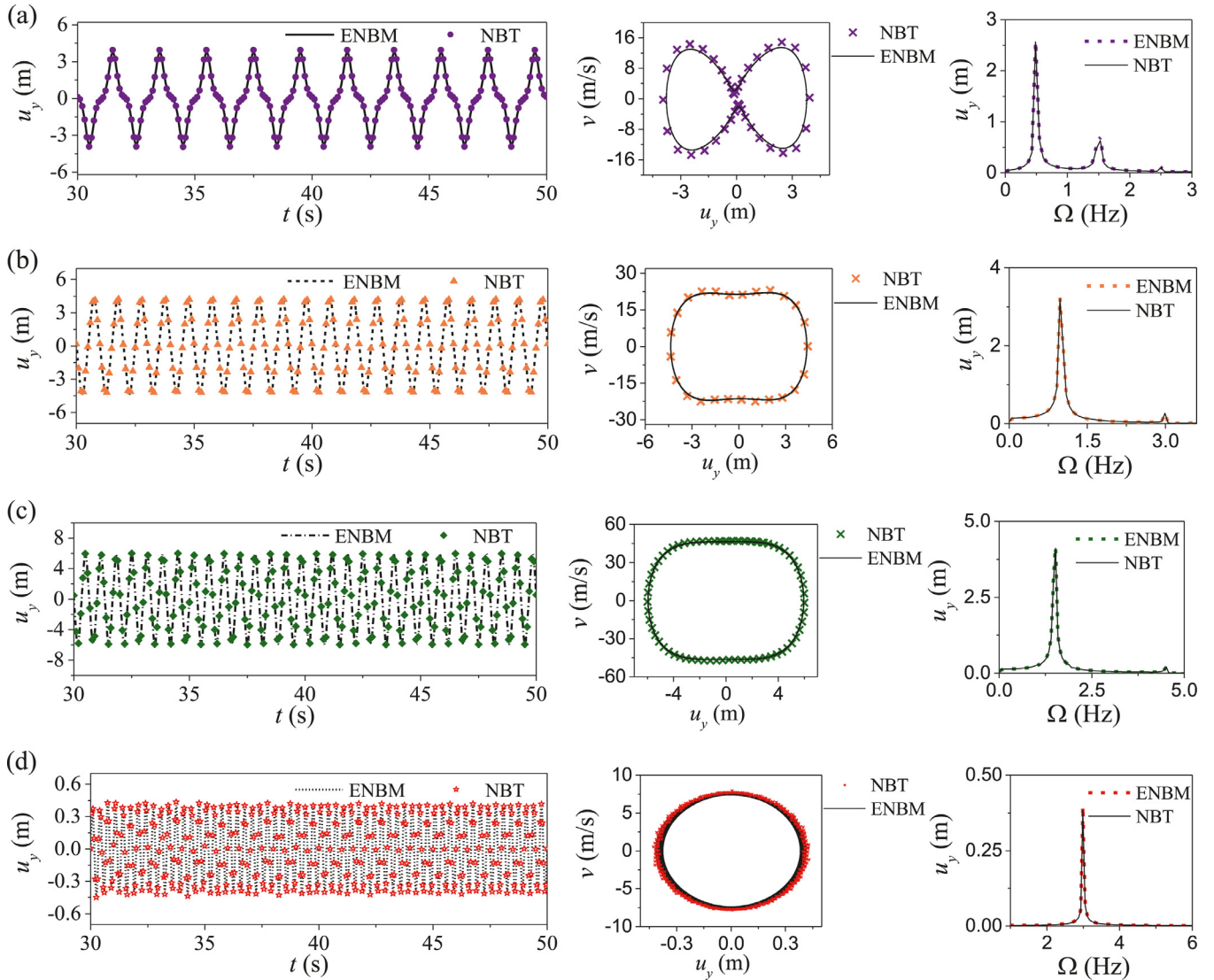


Fig. 10. Comparisons of steady-state responses for the proposed equivalent nonlinear beam model and the nonlinear beamlike truss to check the validity under different external excitation frequencies (a) $\Omega = 0.5\text{Hz}$, (b) $\Omega = 1\text{Hz}$, (c) $\Omega = 1.5\text{Hz}$ and (d) $\Omega = 3\text{Hz}$, for the parameter values $p_0 = 500\text{N/m}$, $c_d = 1.19\text{ N} \cdot \text{s/m}^2$ and $c_r = 2.15\text{ N} \cdot \text{s}$.

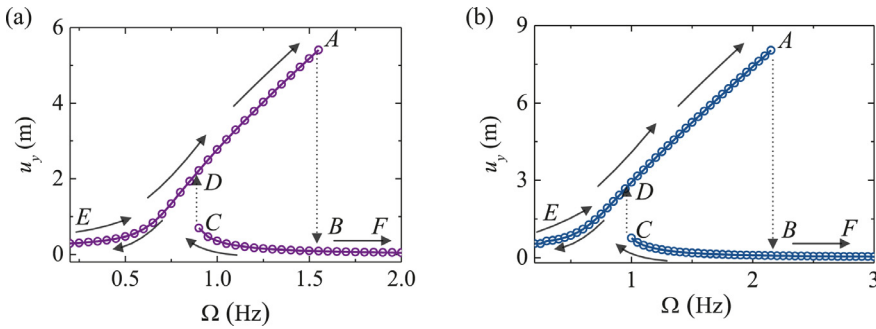


Fig. 11. Frequency-response curves of the equivalent nonlinear beam model under different external excitation magnitudes (a) $p_0 = 25\text{N/m}$ and (b) $p_0 = 50\text{N/m}$, for the parameter values $c_d = 0.5\text{ N} \cdot \text{s/m}^2$, $c_r = 0.5\text{ N} \cdot \text{s}$, where the arrow diagrams in black colour are used for displaying the jump phenomena.

resonance region for the ENBM gradually shifts from the right to the left when damping coefficient becomes larger.

Fig. 13 shows the force-response curve of the ENBM obtained by varying the external force amplitude p_0 as the control parameter. The following parameters are chosen for the numerical calculations: $c_d = 0.3\text{N} \cdot \text{s/m}^2$, $c_r = 0.3\text{N} \cdot \text{s}$ and $\Omega = 1.1\omega_1$. As shown in Fig. 13, the displacement amplitude increases with increasing force amplitude until reaching

point A ($p_0 = 6.5\text{N/m}$), where a limit point bifurcation occurs and the motion becomes unstable. On the contrary, the displacement amplitude will reach the other limit point bifurcation B ($p_0 = 5\text{N/m}$) when decreasing the force amplitude. Beyond one of the limit points, the system is stable periodic response.

The force-response curves of the ENBM for different values of the excitation frequency, namely $\Omega = 0.9\omega_1$, $1.0\omega_1$, $1.1\omega_1$, $1.2\omega_1$ and $1.3\omega_1$,

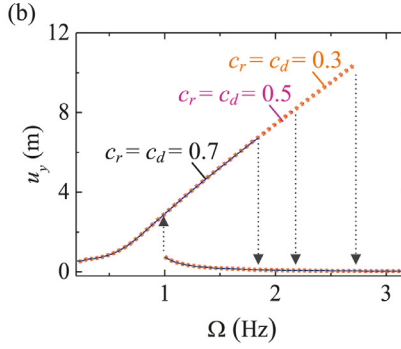
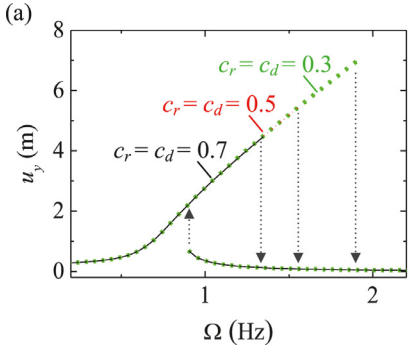


Fig. 12. Effect of the damping on the frequency-response behaviors of the equivalent nonlinear beam model for external excitation magnitudes (a) $p_0 = 25\text{N/m}$ and (b) $p_0 = 50\text{N/m}$ when $c_d = 0.3, 0.5, 0.7\text{N}\cdot\text{s}/\text{m}^2$, $c_r = 0.3, 0.5, 0.7\text{N}\cdot\text{s}$.

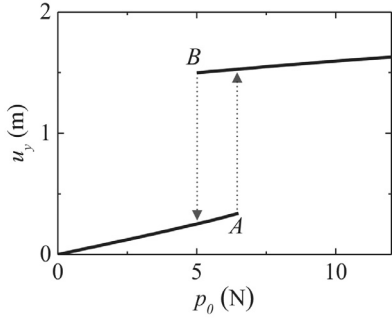


Fig. 13. Force-response curve of the equivalent nonlinear beam model for the parameter values $\Omega = 1.1\omega_1$, $c_d = 0.3\text{N}\cdot\text{s}/\text{m}^2$ and $c_r = 0.3\text{N}\cdot\text{s}$, where the arrow diagram represents bifurcation behavior.

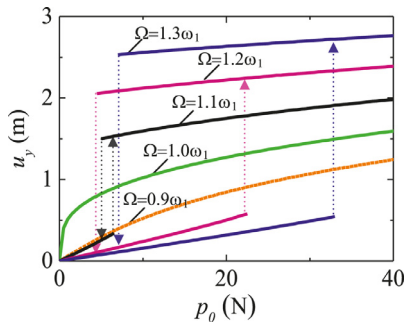


Fig. 14. Variations of the force-response behaviors of the equivalent nonlinear beam model with the excitation frequencies $\Omega = 0.9\omega_1, 1.0\omega_1, 1.1\omega_1, 1.2\omega_1$ and $1.3\omega_1$, where the ω_1 represents the first order linear natural frequency $\omega_1 = 0.75\text{Hz}$, for the parameter values $c_d = 0.3\text{N}\cdot\text{s}/\text{m}^2$, $c_r = 0.3\text{N}\cdot\text{s}$.

are depicted in Fig. 14. It is seen that for $\Omega = 0.9\omega_1$ and $1.0\omega_1$ the system displays only stable periodic responses without any limit point bifurcations. As the excitation frequency increases, limit point bifurcations appear in the force-response curves of the ENBM. The figure reveals that, due to increased excitation frequency, the first limit point bifurcations occur at higher force amplitudes.

Finally, the contribution of the first mode $M = 1$ and the first four order modes $M = 4$ on the nonlinear response of the ENBM is investigated to illustrate the influence of the high order modes on the nonlinear response of the system. For this purpose, the excitation frequency is chosen as the variable parameter and several other system parameters utilized are $p_0 = 25\text{N/m}$, $c_d = 0.1\text{N}\cdot\text{s}/\text{m}^2$, $c_r = 0.1\text{N}\cdot\text{s}$. Numerical simulations have been carried out for the nonlinear system Eq. (24) by varying Ω within the fourth order linear natural frequency, which have been illustrated in Table 2. Selecting the middle point of the ENBM, the results of frequency-response curves for the first mode truncation and fourth mode truncation are represented in Fig. 15. The nonlinear reso-

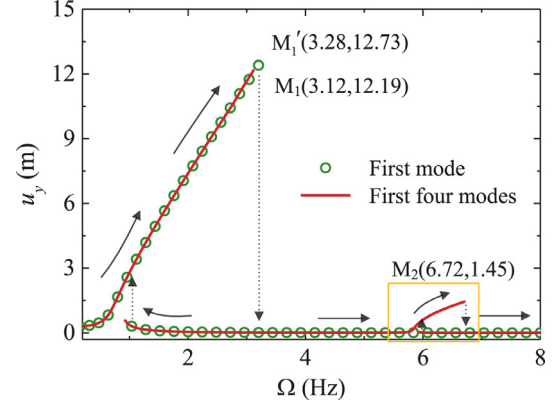


Fig. 15. Influence of the first and first four mode truncations on the frequency-response curves of the equivalent nonlinear beam model, for the parameter values $p_0 = 25\text{N/m}$, $c_d = 0.1\text{N}\cdot\text{s}/\text{m}^2$ and $c_r = 0.1\text{N}\cdot\text{s}$, where green circles and red lines represent first and first four modes responses, respectively.

nance appears near the points M_1 , M'_1 and M_2 , which the corresponding frequencies are $\omega_{1F} = 3.12\text{Hz}$, $\omega_{1F'} = 3.28\text{Hz}$ and $\omega_{3F} = 6.72\text{Hz}$, respectively. As shown in Fig. 15, M'_1 is the resonance peak when selecting the first mode to calculate the frequency-response. However, there exist two resonance peaks M_1 and M_2 for the frequency-response curve obtained from the first four order modes. According to the Table 2, the first and third natural frequencies of the ENBM are, respectively, $\omega_1 = 0.75\text{Hz}$ and $\omega_3 = 5.84\text{Hz}$ for the linear system. It can be found that the first resonance peaks M_1 and M'_1 near the first order frequency, which can indicate that the resonance is mainly caused by the first mode. Obvi-

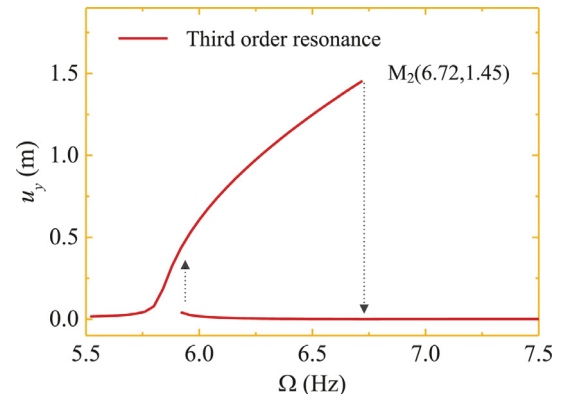


Fig. 16. Frequency-response curve in the frequency range of $\Omega \in (5.5\text{Hz}, 7.5\text{Hz})$ outlined with yellow in Fig. 15, obtained from the first four mode truncation to illustrate the third order resonance region of the equivalent nonlinear beam model.

ously, resonance peak M_2 is close to the third order frequency and results from the third mode. We note that the second and fourth modes have no action on the system response since their modes are nonsymmetrical form. As is evident from Fig. 15, it can be found that the curve bends to higher frequencies in the nonlinear system, which is called hardening response. The vibration amplitudes of the M_1 and M'_1 nonlinear resonance are 12.19m and 12.73m, respectively, and the two resonances are close. The vibration amplitude of M_2 sharp declines after the M_1 and their ratio is 11.89%. Therefore, it can be demonstrated that the primary resonance plays a dominating role in the nonlinear response of the ENBM when the frequency of the external excitation ranges from 0 up to around 5Hz. The third order nonlinear resonance region is shown clearly in Fig. 16. As is evident, the third mode can lead to distinct nonlinear resonance behavior. However, this phenomenon cannot be captured by selecting only the first mode to compute the nonlinear response of the ENBM and cannot be ignored when the frequency of the external excitation is larger than 5Hz.

6. Concluding remarks

With regard to the nonlinear dynamic analysis and the low-order controller design for the beamlike truss, the application of FEM would meet with the computational inefficiency and analytical algorithm inconvenience, especially for large truss structures. In this paper, an efficient equivalent nonlinear beam model (ENBM) is proposed to enhance the vibration control design ability and efficiency of nonlinear response analysis for the nonlinear beamlike truss (NBT). Based on the energy equivalence principle, the ENBM with two pinned ends is established combining the von Karman nonlinear strain-displacement relationship. Taking advantage of the Hamilton principle, the fourth-order nonlinear governing partial differential equations of motion of the ENBM are obtained and solved employing the Galerkin method. To validate the accuracy and efficiency of the proposed ENBM, time histories, phase maps, fast Fourier transform frequency spectrum, linear natural frequency and computational efficiency are studied for both the NBT and the ENBM under different external excitation magnitudes and frequencies. Furthermore, higher modes influence, frequency-response and force-response nonlinear behaviors of the ENBM are investigated to pave the way for future nonlinear study in analytical method.

Numerical calculations are carried out for nonlinear response analysis by using the proposed ENBM and full-scale nonlinear finite element model of the beamlike truss. The main conclusions that can be drawn from this investigation are:

1. Comparisons including time histories, phase maps and fast Fourier transform frequency spectra between results of the ENBM and those obtained from the finite element simulations of the nonlinear beamlike truss have good consistency and satisfied accuracy. The geometric nonlinear response of the beamlike truss can be captured well by the ENBM. The proposed ENBM has important significance for law-order controller design and analytical solution of the NBT.
2. The ENBM can achieve the nonlinear response of the beamlike truss at significantly lower computational costs according to the comparison of computational time to highlight the advantage of the equivalent nonlinear dynamic modeling.
3. From the frequency-response curves, it is found that the ENBM exhibits a hardening-type nonlinear behavior. The influence of the selected mode number on the nonlinear response is studied employing the first order mode and the first four order modes. The results demonstrate that the primary resonance plays a dominating role in the nonlinear response of the ENBM. However, the third order mode can generate non-negligible nonlinear resonance under a certain condition of the external excitation frequency, which cannot be captured by only the first mode to compute the nonlinear response of the ENBM. Furthermore, the frequency-response and the force-response curves of the ENBM reveal that the system possesses

both stable and unstable solution branches, for excitation frequencies more than the first linear natural frequency.

Declaration of Competing Interest

The authors declare that they have no known competing financial interests or personal relationships that could have appeared to influence the work reported in this paper.

CRediT authorship contribution statement

Mei Liu: Conceptualization, Validation, Formal analysis, Writing - original draft, Writing - review & editing. **Dengqing Cao:** Conceptualization, Validation, Formal analysis, Resources, Writing - review & editing, Project administration. **Xiaoyun Zhang:** Validation, Formal analysis, Writing - review & editing. **Jin Wei:** Formal analysis, Writing - review & editing. **Dongfang Zhu:** Conceptualization, Writing - review & editing, Funding acquisition.

Acknowledgments

This research was supported by the National Natural Science Foundation of China (Grant No. 11732005); the Civil Aerospace Project (Grant No. D020213); and the Natural Science Foundation of Shanghai City, PR China (Grant No. 16ZR1415700).

Appendix A. The coefficient expressions of strain and kinetic energy

The coefficient expressions of strain energy for the spatial repeating element in Eq. (1) are

$$\begin{aligned} C_{11} &= \frac{3L_l(2A_dE_dA_lE_lL_b^3 + A_bE_bA_lE_lL_d^3 + 2A_bE_bA_dE_dL_l^3)}{2A_dE_dL_b^3 + A_bE_bL_d^3}, \\ C_{22} = C_{33} &= \frac{A_dE_dL_b^4L_b^2}{2L_d^3} \left(\frac{A_dE_dL_b^3 + A_bE_bL_d^3}{A_bE_bL_d^3 + 2A_dE_dL_b^3} \right) + 3E_lI_{zl}L_l + \frac{1}{2}A_lE_lL_b^2L_l, \\ C_{44} &= \frac{3}{4}G_bJ_bL_b + 3G_lJ_lL_l + \frac{1}{2L_d^3}A_dE_dL_b^4L_l^2, \\ C_{55} = C_{66} &= \frac{3}{L_d^3}A_dE_dL_b^2L_l^2. \end{aligned} \quad (A1)$$

and, the coefficient expressions of kinetic energy for the spatial repeating element in Eq. (2) are

$$\begin{aligned} B_{11} = B_{22} = B_{33} &= \frac{6\rho_dA_d}{L_d^3}(L_b^2L_d^2 + L_b^2L_l^2 + L_l^4) + 3(\rho_bA_bL_b + \rho_lA_lL_l), \\ B_{44} &= L_b^2 \left(\frac{1}{2}\rho_bA_bL_b + \rho_lA_lL_l + \rho_dA_dL_d \right) + 3J_{ol}L_l + \frac{6}{L_d}J_{od}L_l^2, \\ B_{55} = B_{66} &= \frac{1}{4}\rho_bA_bL_b(2L_l^2 + L_d^2) + \frac{1}{4}\rho_lA_lL_l(L_b^2 + L_d^2) \\ &\quad + \frac{1}{2}\rho_dA_dL_d^3 + \frac{3}{2}J_{ob}L_b + \frac{3}{L_d}J_{od}L_b^2. \end{aligned} \quad (A2)$$

where subscript $i = l, b, d$ denotes members of the longerons, the battens and diagonals, respectively. E_iA_i , E_iI_i and G_iJ_i are the extensional, bending and torsional stiffness of the corresponding member, respectively. Also, ρ_iA_i and ρ_iJ_{oi} are the mass and rotational inertia per unit length of the member, respectively. L_i is the length of the member.

References

- [1] Glaesener RN, Lestringant C, Telgen B, Kochmann DM. Continuum models for stretching-and bending-dominated periodic trusses undergoing finite deformations. International Journal of Solids and Structures 2019;171:117–34. doi:[10.1016/j.ijsolstr.2019.04.022](https://doi.org/10.1016/j.ijsolstr.2019.04.022).
- [2] Carlberg K, Ray J, Waanders BB. Decreasing the temporal complexity for nonlinear, implicit reduced-order models by forecasting. Computer Methods in Applied Mechanics and Engineering 2015;289:79–103. doi:[10.1016/j.cma.2015.02.013](https://doi.org/10.1016/j.cma.2015.02.013).

- [3] Goncalves BR, Karttunen AT, Romanoff J. A nonlinear couple stress model for periodic sandwich beams. *Composite Structures* 2019;212:586–97. doi:[10.1016/j.comstruct.2019.01.034](https://doi.org/10.1016/j.comstruct.2019.01.034).
- [4] Malek S, Wierzbicki T, Ochsendorf J. Buckling of spherical cap gridshells: a numerical and analytical study revisiting the concept of the equivalent continuum. *Engineering Structures* 2014;75:288–98. doi:[10.1016/j.engstruct.2014.05.049](https://doi.org/10.1016/j.engstruct.2014.05.049).
- [5] Desmoulins A, Kochmann DM. Local and nonlocal continuum modeling of inelastic periodic networks applied to stretching-dominated trusses. *Computer Methods in Applied Mechanics and Engineering* 2017;313:85–105. doi:[10.1016/j.cma.2016.09.027](https://doi.org/10.1016/j.cma.2016.09.027).
- [6] McCalen D, Romstad K. A continuum model for lattice structures with geometric and material nonlinearities. *Computers & Structures* 1990;37(5):795–822. doi:[10.1016/0045-7949\(90\)90109-F](https://doi.org/10.1016/0045-7949(90)90109-F).
- [7] Zhuang W, Yang C, Wu Z. Modal and aeroelastic analysis of trapezoidal corrugated-core sandwich panels in supersonic flow. *International Journal of Mechanical Sciences* 2019;157:267–81. doi:[10.1016/j.ijmecsci.2019.04.052](https://doi.org/10.1016/j.ijmecsci.2019.04.052).
- [8] Kan Z, Peng H, Chen B, Zhong W. Nonlinear dynamic and deployment analysis of clustered tensegrity structures using a position formulation FEM. *Composite Structures* 2018;187:241–58. doi:[10.1016/j.comstruct.2017.12.050](https://doi.org/10.1016/j.comstruct.2017.12.050).
- [9] Habibi A, Bidmeshki S. A dual approach to perform geometrically nonlinear analysis of plane truss structures. *Steel and Composite Structures* 2018;27(1):13–25. doi:[10.12989/scs.2018.27.1.013](https://doi.org/10.12989/scs.2018.27.1.013).
- [10] Zardi I, Alamatian J. A new formulation for fictitious mass of viscous dynamic relaxation method. *Mechanics Based Design of Structures and Machines* 2019;1:26. doi:[10.1080/15397734.2019.1633342](https://doi.org/10.1080/15397734.2019.1633342).
- [11] Shi H, Salim H. Geometric nonlinear static and dynamic analysis of guyed towers using fully nonlinear element formulations. *Engineering Structures* 2015;99:492–501. doi:[10.1016/j.engstruct.2015.05.023](https://doi.org/10.1016/j.engstruct.2015.05.023).
- [12] Wang CY, Wang RZ, Chuang CC, Wu TY. Nonlinear dynamic analysis of reticulated space truss structures. *Journal of Mechanics* 2006;22(3):199–212. doi:[10.1017/S1727719100000848](https://doi.org/10.1017/S1727719100000848).
- [13] Thai HT, Kim SE. Nonlinear inelastic time-history analysis of truss structures. *Journal of Constructional Steel Research* 2011;67(12):1966–72. doi:[10.1016/j.jcsr.2011.06.015](https://doi.org/10.1016/j.jcsr.2011.06.015).
- [14] Shekastehband B, Ayoubi M. Nonlinear dynamic instability behavior of tensegrity grids subjected to impulsive loads. *Thin-walled Structures* 2019;136:1–15. doi:[10.1016/j.tws.2018.11.031](https://doi.org/10.1016/j.tws.2018.11.031).
- [15] Santana M V, Goncalves P B, Silveira R A. Nonlinear oscillations and dynamic stability of an elastoplastic pyramidal truss. *Nonlinear Dynamics* 2019;98(4):2847–77. doi:[10.1007/s11071-019-05072-9](https://doi.org/10.1007/s11071-019-05072-9).
- [16] Mohit M, Sharifi Y, Tavakoli A. Geometrically nonlinear analysis of space trusses using new iterative techniques. *Asian Journal of Civil Engineering* 2020;1:11. doi:[10.1007/s42107-020-00239-x](https://doi.org/10.1007/s42107-020-00239-x).
- [17] Sohrabi MA, Muliana AH, Srinivasa AR. Controlling deformations of electro-active truss structures with nonlinear history-dependent response. *Finite Elements in Analysis and Design* 2017;129:42–52. doi:[10.1016/j.finel.2017.01.008](https://doi.org/10.1016/j.finel.2017.01.008).
- [18] ElNady K, Goda I, Ganghoffer JF. Computation of the effective nonlinear mechanical response of lattice materials considering geometrical nonlinearities. *Computational Mechanics* 2016;58(6):957–79. doi:[10.1007/s00466-016-1326-7](https://doi.org/10.1007/s00466-016-1326-7).
- [19] Najafgholipour M. An equivalent truss model for in-plane nonlinear analysis of unreinforced masonry walls. *Civil Engineering Journal* 2018;4(4):828–35. doi:[10.28991/cej-0309136](https://doi.org/10.28991/cej-0309136).
- [20] Givois A, Groleau A, Thomas O, Deü JF. On the frequency response computation of geometrically nonlinear flat structures using reduced-order finite element models. *Nonlinear Dynamics* 2019;97(2):1747–81. doi:[10.1007/s11071-019-05021-6](https://doi.org/10.1007/s11071-019-05021-6).
- [21] Jung J, Penning RS, Ferrier NJ, Zinn MR. A modeling approach for continuum robotic manipulators: Effects of nonlinear internal device friction. 2011 IEEE/RSJ International Conference on Intelligent Robots and Systems 2011:5139–46. doi:[10.1109/IROS.2011.6094941](https://doi.org/10.1109/IROS.2011.6094941).
- [22] Liu M, Cao D, Zhu D. Equivalent dynamic model of the space antenna truss with initial stress. *AIAA Journal* 2020;58(4):1851–63. doi:[10.2514/1.J058647](https://doi.org/10.2514/1.J058647).
- [23] Ferretti M. Flexural torsional buckling of uniformly compressed beam-like structures. *Continuum Mechanics and Thermodynamics* 2018;30(5):977–93. doi:[10.1007/s00161-018-0627-9](https://doi.org/10.1007/s00161-018-0627-9).
- [24] Piccardo G, Tubino F, Luongo A. Equivalent nonlinear beam model for the 3-D analysis of shear-type buildings: Application to aeroelastic instability. *International Journal of Non-Linear Mechanics* 2016;80:52–65. doi:[10.1016/j.ijnonlinmec.2015.07.013](https://doi.org/10.1016/j.ijnonlinmec.2015.07.013).
- [25] Piccardo G, Tubino F, Luongo A. Equivalent Timoshenko linear beam model for the static and dynamic analysis of tower buildings. *Applied Mathematical Modelling* 2019;71:77–95. doi:[10.1016/j.apm.2019.02.005](https://doi.org/10.1016/j.apm.2019.02.005).
- [26] D'Annibale F, Ferretti M, Luongo A. Shear-shear-torsional homogenous beam models for nonlinear periodic beam-like structures. *Engineering Structures* 2019;184:115–33. doi:[10.1016/j.engstruct.2019.01.039](https://doi.org/10.1016/j.engstruct.2019.01.039).
- [27] Liu F, Wang L, Jin D, Liu X, Lu P. Equivalent micropolar beam model for spatial vibration analysis of planar repetitive truss structure with flexible joints. *International Journal of Mechanical Sciences* 2020. doi:[10.1016/j.ijmecsci.2019.105202](https://doi.org/10.1016/j.ijmecsci.2019.105202).
- [28] Cao S, Huo M, Qi N, Zhao C, Zhu D, Sun L. Extended continuum model for dynamic analysis of beam-like truss structures with geometrical nonlinearity. *Aerospace Science and Technology* 2020;103:105927. doi:[10.1016/j.ast.2020.105927](https://doi.org/10.1016/j.ast.2020.105927).
- [29] Luongo A, Zulli D. Free and forced linear dynamics of a homogeneous model for beam-like structures. *Mecanica* 2020;55(4):907–25. doi:[10.1007/s11012-019-01070-8](https://doi.org/10.1007/s11012-019-01070-8).
- [30] Stephen NG, Ghosh S. Eigenanalysis and continuum modelling of a curved repetitive beam-like structure. *International Journal of Mechanical Sciences* 2005;47(12):1854–73. doi:[10.1016/j.ijmecsci.2005.07.001](https://doi.org/10.1016/j.ijmecsci.2005.07.001).
- [31] Martin B, Salehian A. Continuum modeling of nonperiodic string-harnessed structures: perturbation theory and experiments. *AIAA Journal* 2019;57(4):1736–51. doi:[10.2514/1.J056615](https://doi.org/10.2514/1.J056615).
- [32] Zhang J, Deng Z, Guo H, Liu R. Equivalence and dynamic analysis for jointed trusses based on improved finite elements. *Proceedings of the Institution of Mechanical Engineers, Part K: Journal of Multi-body Dynamics* 2014;228(1):47–61. doi:[10.1177/1464419313512469](https://doi.org/10.1177/1464419313512469).
- [33] Liu X, Liu H, Du C, Lu P, Jin D, Liu F. Distributed active vibration cooperative control for flexible structure with multiple autonomous substructure model. *Journal of Vibration and Control* 2020;1:1–11. doi:[10.1177/1077546320909968](https://doi.org/10.1177/1077546320909968).
- [34] Casalotti A, D'Annibale F, Rosi G. Multi-scale design of an architected composite structure with optimized graded properties. *Composite Structures* 2020;112608. doi:[10.1016/j.compstruct.2020.112608](https://doi.org/10.1016/j.compstruct.2020.112608).
- [35] Guo J, Xiao Y, Zhang S, Wen J. Bloch wave based method for dynamic homogenization and vibration analysis of lattice truss core sandwich structures. *Composite Structures* 2019;229:111437. doi:[10.1016/j.compstruct.2019.111437](https://doi.org/10.1016/j.compstruct.2019.111437).
- [36] Khakalo S, Niiranen J. Anisotropic strain gradient thermoelasticity for cellular structures: plate models, homogenization and isogeometric analysis. *Journal of The Mechanics and Physics of Solids* 2020;134:103728. doi:[10.1016/j.jmps.2019.103728](https://doi.org/10.1016/j.jmps.2019.103728).
- [37] Jain S, Tiso P. Simulation-free hyper-reduction for geometrically nonlinear structural dynamics: A quadratic manifold lifting approach. *Journal of Computational and Nonlinear Dynamics* 2018;13(7):071003. doi:[10.1115/1.4040021](https://doi.org/10.1115/1.4040021).
- [38] Jain S, Tiso P, Rutzmoser JB, Rixen DJ. A quadratic manifold for model order reduction of nonlinear structural dynamics. *Computers & Structures* 2017;188:80–94. doi:[10.1016/j.compstruc.2017.04.005](https://doi.org/10.1016/j.compstruc.2017.04.005).
- [39] Nampally P, Karttunen AT, Reddy JN. Nonlinear finite element analysis of lattice core sandwich beams. *European Journal of Mechanics A Solids* 2019;74:431–9. doi:[10.1016/j.euromechsol.2018.12.006](https://doi.org/10.1016/j.euromechsol.2018.12.006).
- [40] Karttunen AT, Reddy JN, Romanoff J. Two-scale constitutive modeling of a lattice core sandwich beam. *Composites Part B: Engineering* 2019;160:66–75. doi:[10.1016/j.compositesb.2018.09.098](https://doi.org/10.1016/j.compositesb.2018.09.098).
- [41] Pal RK, Ruzzene M, Rimoli JJ. A continuum model for nonlinear lattices under large deformations. *International Journal of Solids and Structures* 2016;96:300–19. doi:[10.1016/j.ijsolstr.2016.05.020](https://doi.org/10.1016/j.ijsolstr.2016.05.020).
- [42] El Nady K, Dos Reis F, Ganghoffer J. Computation of the homogenized nonlinear elastic response of 2D and 3D auxetic structures based on micropolar continuum models. *Composite Structures* 2017;170:271–90. doi:[10.1016/j.compstruc.2017.02.043](https://doi.org/10.1016/j.compstruc.2017.02.043).
- [43] Duan S, Wen W, Fang D. A predictive micropolar continuum model for a novel three-dimensional chiral lattice with size effect and tension-twist coupling behavior. *Journal of The Mechanics and Physics of Solids* 2018;121:23–46. doi:[10.1016/j.jmps.2018.07.016](https://doi.org/10.1016/j.jmps.2018.07.016).
- [44] Arabnejad S, Pasini D. Mechanical properties of lattice materials via asymptotic homogenization and comparison with alternative homogenization methods. *International Journal of Mechanical Sciences* 2013;77:249–62. doi:[10.1016/j.ijmecsci.2013.10.003](https://doi.org/10.1016/j.ijmecsci.2013.10.003).
- [45] Ilchev A, Macardon V, Kruch S, Forest S. Computational homogenisation of periodic cellular materials: application to structural modelling. *International Journal of Mechanical Sciences* 2015;93:240–55. doi:[10.1016/j.ijmecsci.2015.02.007](https://doi.org/10.1016/j.ijmecsci.2015.02.007).
- [46] Philipot G, Kochmann DM. A quasicontinuum theory for the nonlinear mechanical response of general periodic truss lattices. *Journal of The Mechanics and Physics of Solids* 2019;124:758–80. doi:[10.1016/j.jmps.2018.11.014](https://doi.org/10.1016/j.jmps.2018.11.014).
- [47] Qiu K, Wang R, Wang Z, Zhang W. Effective elastic properties of flexible chiral honeycomb cores including geometrically nonlinear effects. *Mecanica* 2018;53(15):3661–72. doi:[10.1007/s11012-018-0911-6](https://doi.org/10.1007/s11012-018-0911-6).
- [48] Chowdhury S R, Reddy J N. Geometrically exact micropolar Timoshenko beam and its application in modelling sandwich beams made of architected lattice core. *Composite Structures* 2019;226:111228. doi:[10.1016/j.compstruct.2019.111228](https://doi.org/10.1016/j.compstruct.2019.111228).
- [49] Ghayesh MH, Amabili M, Farokhi H. Nonlinear forced vibrations of a microbeam based on the strain gradient elasticity theory. *International Journal of Engineering Science* 2013;63(63):52–60. doi:[10.1016/j.ijengsci.2012.12.001](https://doi.org/10.1016/j.ijengsci.2012.12.001).
- [50] Ghayesh MH, Farokhi H, Amabili M. Nonlinear dynamics of a microscale beam based on the modified couple stress theory. *Composites Part B: Engineering* 2013;50:318–24. doi:[10.1016/j.compositesb.2013.02.021](https://doi.org/10.1016/j.compositesb.2013.02.021).
- [51] Ansari R, Gholami R, Sahmani S. Study of small scale effects on the nonlinear vibration response of functionally graded Timoshenko microbeams based on the strain gradient theory. *Journal of Computational and Nonlinear Dynamics* 2012;7(3):031009. doi:[10.1115/1.4006040](https://doi.org/10.1115/1.4006040).
- [52] Ansari R, Shojaei MF, Mohammadi V, Gholami R, Sadeghi F. Nonlinear forced vibration analysis of functionally graded carbon nanotube-reinforced composite Timoshenko beams. *Composite Structures* 2014;113(113):316–27. doi:[10.1016/j.compstruct.2014.03.015](https://doi.org/10.1016/j.compstruct.2014.03.015).
- [53] Farokhi H, Ghayesh MH, Amabili M. Nonlinear dynamics of a geometrically imperfect microbeam based on the modified couple stress theory. *International Journal of Engineering Science* 2013;68:11–23. doi:[10.1016/j.ijengsci.2013.03.001](https://doi.org/10.1016/j.ijengsci.2013.03.001).
- [54] Asghari M, Kahrobaiany M, Ahmadian M. A nonlinear Timoshenko beam formulation based on the modified couple stress theory. *International Journal of Engineering Science* 2010;48(12):1749–61. doi:[10.1016/j.ijengsci.2010.09.025](https://doi.org/10.1016/j.ijengsci.2010.09.025).
- [55] Arbind A, Reddy J. Nonlinear analysis of functionally graded microstructure-dependent beams. *Composite Structures* 2013;98:272–81. doi:[10.1016/j.compstruct.2012.10.003](https://doi.org/10.1016/j.compstruct.2012.10.003).
- [56] Reddy J. Microstructure-dependent couple stress theories of functionally graded beams. *Journal of the Mechanics and Physics of Solids* 2011;59(11):2382–99. doi:[10.1016/j.jmps.2011.06.008](https://doi.org/10.1016/j.jmps.2011.06.008).

- [57] Yan T, Yang J, Kitipornchai S. Nonlinear dynamic response of an edge-cracked functionally graded Timoshenko beam under parametric excitation. *Nonlinear Dynamics* 2012;67(1):527–40. doi:[10.1007/s11071-011-0003-9](https://doi.org/10.1007/s11071-011-0003-9).
- [58] Ke LL, Yang J, Kitipornchai S. Nonlinear free vibration of functionally graded carbon nanotube-reinforced composite beams. *Composite Structures* 2010;92(3):676–83. doi:[10.1016/j.compstruct.2009.09.024](https://doi.org/10.1016/j.compstruct.2009.09.024).
- [59] Foda MA. Influence of shear deformation and rotary inertia on nonlinear free vibration of a beam with pinned ends. *Computers & Structures* 1999;71(6):663–70. doi:[10.1016/S0045-7949\(98\)00299-5](https://doi.org/10.1016/S0045-7949(98)00299-5).
- [60] Zhang W, Chen J, Zhang Y, Yang X. Continuous model and nonlinear dynamic responses of circular mesh antenna clamped at one side. *Engineering Structures* 2017;151:115–35. doi:[10.1016/j.engstruct.2017.08.013](https://doi.org/10.1016/j.engstruct.2017.08.013).